Surface-sensitive conductance measurements

2009 J. Phys.: Condens. Matter 21 013003

(http://iopscience.iop.org/0953-8984/21/1/013003)

J. Phys.: Condens. Matter **21** (2009) 013003 (21pp) doi:10.1088/0953-8984/21/1/013003

TOPICAL REVIEW

Surface-sensitive conductance measurements

Ph Hofmann[1] **and J W Wells**[2]

Institute for Storage Ring Facilities (ISA) and Interdisciplinary Nanoscience Center (iNANO), University of Aarhus, 8000 Aarhus C, Denmark

E-mail: philip@phys.au.dk

Received 25 June 2008, in final form 22 September 2008
Published 1 December 2008
Online at stacks.iop.org/JPhysCM/21/013003

Abstract
Several approaches for surface-sensitive conductance measurements are reviewed. Particular emphasis is placed on nanoscale multi-point probe techniques. The results for two model systems, which have given rise to some dispute, are discussed in detail: Si(111)(7 × 7) and ($\sqrt{3} \times \sqrt{3}$)Ag–Si(111). Other recent examples are also given, such as phase transitions in quasi-one-dimensional structures on semiconductor surfaces and the surface sheet conductivity of Bi(111), the surface of a semimetal.

(Some figures in this article are in colour only in the electronic version)

Contents

[1] Present address: Surface Science Research Centre, University of Liverpool, UK.
[2] Present address: Norwegian University of Science and Technology (NTNU), 7491 Trondheim, Norway.

1. Introduction

The conductivity of a solid is one of its most basic physical properties. Its value and temperature dependence are often used to classify solids as metals, semiconductors and insulators. Conductivity changes frequently herald interesting effects such as superconductivity, charge density waves and magnetoresistance. Despite its paramount importance to bulk solid state physics, relatively little is known about the conductivity of surfaces, mostly due to the experimental difficulties associated with the measurement.

There are good reasons to believe that electric transport on surfaces is interesting. First of all, many surfaces support localized electronic states, which could cause the surface electronic properties to be different from those of the bulk. Moreover, the two-dimensional character of these electronic surface states offers a good experimental opportunity to study transport in a two-dimensional system. Finally, the surface of a solid is easy to modify, for example by adsorbing self-ordering layers of atoms or (organic) molecules. This opens virtually infinite possibilities to construct a structure with the desired properties for conduction, sensing, switching and so on.

If the surface of a solid has different electronic properties from the bulk, this leads to a simple picture for the current flow near the surface. The entire system can be thought of as a two-dimensional sheet, with a certain (surface) conductivity,

and the underlying semi-infinite bulk, which has a different conductivity. If two contacts are attached to the surface, the current path between them mainly depends on two quantities: the ratio of bulk to surface conductivity and the distance between the contacts. If the contact distance is large, the current will spread out deeply into the bulk and the surface sensitivity of the measurement will be minimal. The same problem will arise if the bulk is much more conductive than the surface. As we shall see, surface sensitivity can currently only be achieved when using very small contact spacings on poorly conducting bulk samples (e.g. on semiconductors). Even then, it can be difficult to extract the surface *conductivity* from the measured *conductance*, which contains both surface and bulk contributions.

In practice, it turns out that surface-sensitive conductance measurements are frequently performed with four contacts to the surface, not two. The reason for this is the same as in the case of bulk conductance measurements. When only two contacts are used, the measured resistance contains contributions from the probes and the contacts, which can be large and non-ohmic. This problem is solved by using four contacts, two to supply the current and two to measure the voltage drop without draining any current. However, the above consideration for contact spacings applies for four contacts as well as for two contacts: in order to achieve surface sensitivity, the contact spacing has to be very small in most cases.

The development of conductance probes with ever smaller contact distances also opens the possibility for conductance measurements on micro- or nanoscale structures such as nanowires, nanotubes or other artificially constructed devices. To this end, a nanoscale conductance probe has to be combined with a microscopic technique, such as a scanning electron microscope.

In this paper, we will review the short history of surface and nanoscale conductance measurements. We will present different techniques which can be used and we will discuss a number of cases, starting from conduction through simple, clean surfaces to adsorbed layers and thin films. Before turning to surface conductivity, we briefly address two fundamental issues. The first is why one can expect surface conductivity to be interesting and the second is the conceptual difficulties associated with measuring it.

2. Surface electronic properties

2.1. Clean and adsorbate-covered surfaces: prospects for conductance measurements

In this section, we briefly describe the surface electronic properties of different systems and discuss their potential interest for surface conductance measurements. We also clarify what we mean by a surface being 'metallic' or 'semiconducting' and we discuss what can be expected for the conductance of semiconductor surfaces.

Even for clean, unreconstructed metal surfaces, the surface electronic properties can be quite different from those of the bulk and one should therefore also expect the transport properties to be different. The simplest and oldest examples are the free-electron-like electronic surface states on the surfaces of simple and noble metals [1–11], which are caused by the termination of the bulk. Being found on the surfaces of very good bulk conductors, there can be little hope to directly measure conductance through these surface states (see later sections), but, on the other hand, there is no question that these surfaces as such can be termed 'metallic' in the sense of supporting surface states with a well defined Fermi contour.

A more recent example of clearly metallic surface states is the surfaces of bismuth, a semimetal [12–15]. Due to the relatively low density of bulk carriers in Bi and the high density of surface states, a direct measurement of transport though them could be achievable. We return to this case later.

The adsorption of molecules or thin metal films on a metal surface can have a pronounced impact on the surface electronic structure. It can change the surface states already present [16] and it can induce new states caused by the adsorbates [17–19] or quantum well states [20, 21]. The properties of thin metal films on metals can be particularly interesting because of the question of whether these films behave as metals or semiconductors [22, 23]. Again, a direct measurement of the conductance through adsorbates or ultra-thin metal layers on the surface of a well conducting metal surface is not practical at present, and these systems will not therefore be discussed in any further detail here.

The clean or adsorbate-covered surfaces of semiconductors and insulators are more promising candidates for a direct measurement of surface conductance due to the poor conduction through the bulk. In fact, all but one of the examples described in the later sections of this paper refer to the surfaces of semiconductors. If we suppose for a moment that the conduction though the bulk semiconductor can be totally neglected (for a detailed discussion of this problematic assumption see the end of this section), what to expect for the surface remains an interesting question.

The creation of a surface on a semiconductor typically leads to cut or dangling sp^3 bonds. In a band picture, having an odd number of such dangling bonds per surface unit cell should give rise to metallic surface states. In contrast to this, most semiconductor surfaces do not support metallic surface states. In fact, the surface structure often undergoes major reconstruction in order to avoid a metallic surface. Often the character of the reconstruction is to remove dangling bonds and turn the surface into a band insulator [24].

There are, however, a number of more interesting cases in which the electronic character of the surface shows reversible temperature-dependent phase transitions [25] and/or where it is dominated by many-body effects. Quite generally, such scenarios are likely when the surface periodicity and electron counting predict a metallic surface but with narrow bands (low kinetic energy), strong Coulomb repulsion and/or strong electron–phonon coupling. Much studied model systems for such transitions are the hexagonal surfaces of Si(111), Ge(111) and SiC(0001) or SiC(111) with a third of a monolayer of group IV atoms adsorbed in the so-called T_4 sites. Some of these systems have complicated phase diagrams with several reversible phase transitions [26, 27] but a low temperature ground state which appears to be a Mott insulator [28–30]. More stable Mott insulating

phases are found for the $\sqrt{3} \times \sqrt{3}$ surface termination of SiC(0001) [31–34] and for K/Si(111):B [35]. To the best of our knowledge, none of these systems have so far been studied by conductance measurements.

For some semiconductor surfaces, notably Si(111)(7 × 7), the electronic character is not entirely clear yet. Electron counting would again suggest a metallic surface but the distances are so large that the bandwidth could be expected to be very narrow and thus correlation effects to be important. Experimentally, Si(111)(7 × 7) appears to show a Fermi surface [36] with rather strong electron–phonon coupling [37] and an electron energy loss peak consistent with a metallic surface [38] at room temperature. NMR experiments, on the other hand, have suggested that the surface is close to a Mott–Hubbard metal insulator transition [39]. A detailed review of conductance measurements on Si(111)(7 × 7) is given in the present paper.

Semiconductor surfaces would also be important substrates for the electrical characterization of ultra-thin metal films showing quantum size effects [20, 21]. One could expect the conductance to show oscillations as a function of thickness, caused by the variations of the density of states at the Fermi level. It might even be possible to directly probe oscillations in the critical temperature for a superconducting state, if present [40].

Semiconductor surfaces with a controlled step density have been shown as suitable substrates for the growth of highly ordered quasi-one-dimensional structures [41, 42]. One-dimensional metals are interesting because they can be expected to be particularly susceptible to phenomena such as metal–insulator transitions (Peierls type, Mott type), the formation of a Luttinger liquid or spin–charge separation [43–46]. A much studied example is the Si(553)–Au atomic chain structure [47–49], for which a metal–insulator transition is indeed observed [50]. The conductivity of other systems, In chains on Si(111) and the Pb induced chain structures on Si(557), will be reviewed in this paper.

Finally, it would be interesting to study electronic transport through self-organized molecular nanostructures. Such systems hold fascinating prospects for future electronics. Evidently, they cannot be free standing but would have to be placed on a substrate. As in the previous cases, the substrate of choice would be a semiconductor or an insulator, not a metal. This, however, holds some challenges.

The self-organized structure of many large organic molecules has been studied in great detail by scanning tunnelling microscopy (STM) [51–54]. Most of this research has been carried out on metal surfaces because these can be viewed as an (electronically) flat template for the growth, in the sense of having a smooth, low-corrugation charge density and no dangling bonds. The molecule–substrate interaction is weak and the molecules order due to their mutual interaction. Particularly promising molecules for building self-organized layers are phthalocyanine or porphyrin based [55] or of the so-called 'Lander' type. The latter consist of a π-system which is de-coupled from the surface by molecular 'legs' [56, 57].

On semiconductors, especially on group IV materials, molecular ordering is more difficult to achieve because of the much stronger molecule–substrate interaction, especially through the dangling bonds often present on semiconductor surfaces [53, 58]. On Si(111) several studies have shown that this problem can be solved by depositing one monolayer of silver atoms on the surface and thereby saturating all dangling bonds [59–62]. In this way, the advantages of a metal and a semiconductor surface are combined. The molecule–substrate interaction is substantially reduced, self-ordering can be achieved and, at the same time, the electronic structure of both substrate and surface is that of a semiconductor or a semimetal [63]. A direct measurement of the conductance of adsorbed molecular monolayers is, to the best of our knowledge, not reported anywhere.

2.2. Is the surface metallic?

In connection with conductance measurements, an important question will be if a surface is metallic or semiconducting/insulating. At first glance, this might seem trivial but it turns out to be a major source of confusion and it is important that we clarify what we mean by the term 'metallic' in the first place. A brief discussion of the aspects related to conductivity is given here. An excellent broader review, including a detailed discussion of how the metallic or non-metallic character of surfaces can be probed by spectroscopic techniques, is found in [23].

From a conductivity point of view, conventional wisdom has it that metals are 'good' conductors. But with the conductivity of different solids spanning more than 20 orders of magnitude, it is not clear what 'good' actually is. In any case, one would expect a metallic surface to have a reasonably high conductivity. A possible approach to classifying a surface as a metal is thus to consider the absolute value of the surface conductivity. One can compare it with the minimum value for metallic conductivity in two dimensions following the Ioffe–Regel criterion, which is $3.83 \times 10^{-5}\ \Omega^{-1}$ [64].

Another frequently used criterion is the temperature dependence of the conductivity. It is often assumed that the conductivity for a semiconductor increases as the temperature is raised (because of the increased number of carriers) whereas it decreases for metals (because of the increased electron–phonon interactions). This, however, is rather problematic because its validity for a semiconductor depends on the doping and on the temperature. Using this criterion, moderately doped bulk silicon, for example, exhibits a 'metallic' temperature dependence of the conductivity near room temperature. There are even metals which do not obey the rule, such as liquid zinc [65, 66] or systems showing the Kondo effect [67].

An alternative criterion for surface metallicity can be the presence of a finite density of states at the Fermi level or, equivalently, no minimum energy for the creation of electron–hole pairs. This can be probed by spectroscopic techniques such as (inverse) photoemission, tunnelling spectroscopy or electron energy loss spectroscopy. But this criterion, too, can be problematic because the states giving rise to this density of states at the Fermi level could be very localized. Thus, the metallicity of a surface has to be discussed in terms of both the density of states at the Fermi level and the conductivity.

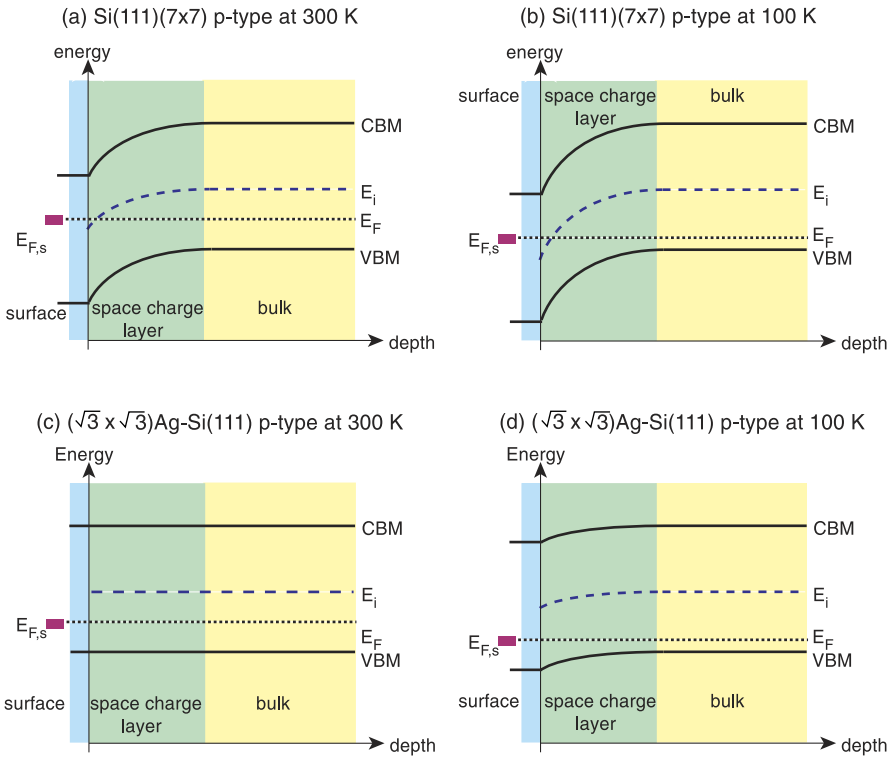

Figure 1. Band bending near the surface of a p-doped Si(111) wafer for two terminations ((7 × 7) and ($\sqrt{3} \times \sqrt{3}$)Ag) and at two temperatures. CBM and VBM denote the conduction band minimum and valence band maximum, respectively. E_{i} is the intrinsic level, $E_{\mathrm{F,s}}$ the surface Fermi level and E_{F} the bulk Fermi level.

2.3. What determines the conductance of a semiconductor surface?

Some of the apparent contradictions reported in the literature on the surface conductivity of semiconductors are at least partly due to different definitions of the surface conductivity. Therefore, we briefly address this issue here.

The objective of most experiments is to study the conductivity of the surface as such, i.e. the conduction through electronic surface states, through surface states modified by adsorption or through ultra-thin layers of atoms or molecules on the surface. A measurement of voltage and current does, however, not yield the *conductivity* of a system but merely the *conductance*. The conductance measured from a solid surface contains contributions from the surface as such and from the underlying solid. Extracting the surface conductivity from the measurement can be non-trivial.

In most conductance measurements, and in particular in those with four-point probes, the penetration of the current into the bulk solid depends on the detailed geometry of the experiment. For a collinear four-point probe, we shall see that the measured conductance is independent of the probe spacing for a purely two-dimensional system and proportional to the contact spacing for the semi-infinite bulk. Naïvely, one could expect the measured conductance of a solid to be the sum of the surface and the bulk conductance. For a macroscopic contact spacing, the bulk conductance would then dominate the measurement, as expected.

Although it is tempting to attribute any 'non-bulk' contribution to the measured conductance as being due to the surface, the situation is, unfortunately, much more complex for semiconductor surfaces due to the existence of a space-charge layer near the surface. The carrier density in the space-charge layer is different from that in the bulk and it depends on the depth below the surface. The character of the space charge layer, in turn, depends on the temperature, the bulk doping of the semiconductor and on the position of the Fermi level at the surface. All this is well known (see for example [68]) but not always taken properly into account in surface conductance measurements. A detailed account of the physics of the space-charge layer is given in [64, 69].

To make matters worse, the position of the surface Fermi level, and therefore the entire band bending and space-charge layer situation, depends on the detailed surface electronic structure, i.e. on the electronic properties of the clean surface or on the presence, type and structure of adsorbates on the surface. It is therefore insufficient to measure or calculate the space-charge layer conductance of the clean surface in order to subtract its value from that of the adsorbate-covered surface, or in order to use it as an argument that the space-charge layer contribution is insignificant. Instead, one has to make sure that the space-charge layer contribution remains insignificant for the entire experiment, i.e. for all adsorbates and temperatures. If the surface Fermi level for the system under investigation is known, one can at least numerically simulate the expected contribution of the space-charge layer to the measurements [70].

The level of complexity arising from these considerations is illustrated in figure 1, which shows the temperature-

dependent band bending for two surface terminations of p-doped Si(111), clean (7 × 7) and ($\sqrt{3} \times \sqrt{3}$)Ag. In both cases the Fermi level at the surface $E_{F,s}$ is pinned by a high density of surface states, for Si(7 × 7) above mid-gap [71] and for ($\sqrt{3} \times \sqrt{3}$)Ag–Si(111) close to the valence band maximum [72–74, 63, 75]. The position of the bulk Fermi level E_F in a doped semiconductor is strongly temperature dependent and it can be very different from the intrinsic value E_i. If the bulk doping is known, its position can be calculated and the depth-dependent band bending is obtained from the bulk and the surface Fermi level position [68, 64].

The band bending near the Si(111)(7 × 7) and ($\sqrt{3} \times \sqrt{3}$)Ag terminations is very different. At room temperature Si(111)(7 × 7) shows a down-bending of the valence band with respect to the Fermi level towards the surface. In the p-doped sample this corresponds to a carrier depletion near the surface. In contrast to this, ($\sqrt{3} \times \sqrt{3}$)Ag shows hardly any band bending, such that the carrier concentration is almost independent of the distance from the surface. One might thus expect that the space-charge layer of ($\sqrt{3} \times \sqrt{3}$)Ag is far more conductive than that of (7 × 7), leading to a higher conductance through space charge layer and bulk. In the case of a four-point probe with a contact spacing of 10 μm or so, this turns out *not* to be the case: the space-charge layer of (7 × 7) is sufficiently conductive at room temperature and one would expect to measure approximately the same conductance for the two surfaces. At low temperature the band bending increases in both cases. For (7 × 7) it is now very strong, leading to weak inversion at the surface and to an effectively insulating space-charge layer. For ($\sqrt{3} \times \sqrt{3}$)Ag, in contrast, it is still small, smaller than for (7 × 7) at room temperature. Consequently, the space-charge layer contribution to the conductance drops by many orders of magnitude when cooling (7 × 7) from room temperature to 100 K but it remains almost constant for ($\sqrt{3} \times \sqrt{3}$)Ag.

The bottom line is that the conductance contribution through the bulk and the space-charge layer depends on the distance between the contacts in a multi-point probe measurement, on the type and level of doping, on the temperature and on the surface termination. The dependence on any of these parameters can be very strong given the steepness of the Fermi–Dirac distribution which governs the carrier concentration. It is, in general, insufficient to estimate the conductivity of the space charge layer for a particular situation, and a rigid numerical treatment is required.

3. Techniques for surface-sensitive conductance measurements

The objective of a surface-sensitive transport measurement must be the determination of the two-dimensional (2D) conductivity σ_s which is due to the electronic surface states. Being a genuine sheet conductivity, this quantity has the dimension of a conductance (i.e. the unit 1 S = 1 Ω^{-1}), unlike the usual three-dimensional (3D) bulk conductivity, which has the dimension of a conductance per length (i.e. the unit 1 S m^{-1} = 1 Ω^{-1} m^{-1}). Instead of merely using Ω^{-1}, two-dimensional conductivity is also often expressed as Ω^{-1} per square or $\Omega^{-1}/\square$ in order to distinguish it from conductance.

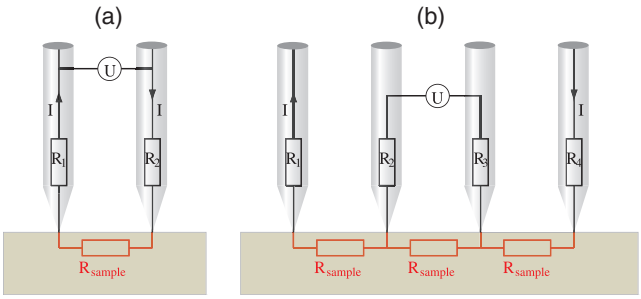

Figure 2. Sketch of (a) a two-point probe and (b) a collinear four-point probe with equi-distant contact spacing. Wire and contact resistances are symbolized by $R_1 \cdots R_4$ and the sample resistance by R_{sample}.

A general difficulty is, of course, that the measured conductance contains contributions from the surface, the space-charge layer and the bulk, and these have to be disentangled. How this can be achieved is discussed in the following. As a starting point, it is useful to stick to a model made up from the two limiting cases: a solid surface is thought to consist of a semi-infinite bulk with a conductivity of σ_b and a two-dimensional surface with conductivity σ_s. The additional, and possibly considerable, complication of the space-charge layer is addressed later.

Perhaps the most used conductance probe is a simple multimeter. By measuring the potential between two contacts when a known current is applied, it seems trivial to find the resistance of a sample. However, the major drawback of this method is that the measurement will intrinsically include the series resistance of the wires and contacts. The situation is schematically shown in figure 2, which illustrates that it is impossible to infer the resistance of the sample R_{sample} when measuring the voltage drop and current with merely two contacts. The result always contains the resistance of the wires and the contacts, symbolized by R_1 and R_2. The problem can be solved by using a four-point probe. This approach is described in detail later in this paper. In short, if the voltage drop over the inner two contacts can be measured without draining any current, this voltage drop divided by the current through the outer contacts is a measure of the sample resistance only. The total current is, of course, still influenced by the resistance of the two outer contacts, but this resistance becomes irrelevant because it is the current which is controlled and not the voltage to the outer contacts.

On a macroscopic scale, the problem of wire and contact resistance in a two-point probe is usually circumvented by ensuring that the resistance of the cables and contacts is insignificant relative to the resistance of the sample. In some cases this is already problematic, for example for metallic probes on a semiconducting sample, where the metal–semiconductor interface can give rise to a Schottky diode type contact, thus making the contact resistance large and non-ohmic. Additionally, when nanoscale measurements are required, the physical size of the probes must be reduced, and this results in an increased resistance of the probes and cables.

3.1. One-, two- and three-contact measurements

Although measurements with one and two contacts have limitations, with careful application they can be very useful. A one-contact measurement would typically be made by the tip of an STM such that the surface conductivity would somehow be inferred from the measured tunnelling conductance. While describing this as a one-contact measurement, it is of course assumed that there is a second, macroscopic contact to the sample in order to have a closed circuit. Two contacts can potentially measure the surface conductance but suffer from the restrictions discussed qualitatively above. Three contacts could have all the advantages of four, if the current is supplied by two of them and the last is movable in order to map out the potential across the surface. We start by briefly outlining the theory behind two-contact measurements, and discuss instruments and measurements which use this, and similar, principles.

First, it is useful to state how the measured resistance U/I is related to σ_s and σ_b for purely 2D and 3D cases, respectively, in the ideal situation of $R_1 = R_2 = 0$ (see figure 2). The potential in the sample in the vicinity of a single contact is described by the Poisson equation

$$\nabla(\sigma(\mathbf{r})\nabla\Phi(\mathbf{r})) = 0, \tag{1}$$

where $\sigma(\mathbf{r})$ is the conductivity of the sample. The equation is written in a more general form than the usual $\nabla^2\Phi(\mathbf{r}) = 0$ in order to allow for a spacial variation of the sample's conductivity.

For a homogeneous, semi-infinite three-dimensional (3D) conductor, (1) can be solved analytically. The two contacts are both held at a fixed potential and the potential around each contact can be evaluated. Thus, it is possible to infer the potential difference between the contacts for a given current between them. The measured two-point sample resistance R_{3D}^{2pp} is defined as U/I and one easily obtains

$$R_{3D}^{2pp} = \frac{U}{I} = \frac{1}{\pi\sigma_b}\left(\frac{1}{r} - \frac{1}{s-r}\right), \tag{2}$$

where s is the spacing between the contacts and r the radius of the contacts, which are assumed to be made of a metal with infinite conductivity [76].

In the case of a homogeneous and infinite 2D conductor the same calculation can be made, starting from the 2D version of the Poisson equation, yielding

$$R_{2D}^{2pp} = \frac{U}{I} = \frac{1}{\pi\sigma_s}\ln\left(\frac{s-r}{r}\right). \tag{3}$$

Note that it is not possible to determine the expected resistance values for point contacts. Thus, some assumptions about the size and shape of the contacts are required.

Conductivity measurements on Si(111) using two STM tips *in the tunnelling regime* were reported by Jaschinsky *et al* [76]. While this approach is new and still needs further development and analysis, it has become clear that the problem arising from the contact resistance can be circumvented elegantly by varying the distance of the STM tips from the surface and making use of the fact that the contact resistance depends exponentially on the sample–tip separation.

Different strategies for one-contact measurements of surface conductance have been tried using an STM tip, either in true contact or in the tunnelling regime. In fact, the STM always measures a conductance—since the potential difference between tip and sample V and the tunnelling current I are both known. The (differential) conductance is simply described by $\mathrm{d}I/\mathrm{d}V$. However, this is strictly the conductance of the tunnel junction and it is not directly related to σ_s or σ_b.

An approach for the determination of σ_s by STM along these lines has been suggested by Hasegawa *et al* [77]. When studying the current versus voltage characteristics of an STM tip in contact with a clean Si surface, they found a qualitative agreement with the expected Schottky barrier for a metal–semiconductor contact. A quantitative analysis, however, showed that the conductance at zero bias and in the reverse-bias direction was much larger than the expected value. Moreover, it depended strongly on the surface cleanliness and morphology, i.e. it was different for oxygen-covered surfaces and on small islands, but it did not depend on the bulk doping. This led the authors to propose that the excess conductance at zero bias voltage could be identified with the surface state conductance. If one assumes that the extra current is entirely carried by the surface states, a surface sheet conductivity of the order of $10^{-6}\ \Omega^{-1}$ must be present.

An alternative approach to conductance measurements by STM was suggested by Heike *et al* and their result is shown in figure 3. The basic idea behind the experiment is that the tunnelling current has to flow away from the tip and it can do so via different paths. In our simple picture of only bulk and surface conductivity σ_b and σ_s, this can happen either directly into bulk states or laterally through electronic surface states. Information about the surface state conductivity can thus be obtained by partly blocking the latter path. This blocking is achieved by using the STM tip to fabricate a trench in the surface. Figure 3(a) shows an example of such a trench around a tongue of pristine Si(111)(7 × 7). The figure also shows the brightness change along the length of the tongue which reflects a potential difference due to a resistance: for electrons which tunnel into the apex of the tongue, the path away from the tip is more resistive than for electrons entering at the base of the tongue, because they have to pass through the entire length of the tongue. The data are analysed by fitting the measured voltage drop along the tongue to a simple model network of resistors as shown in 3(c) and the surface sheet conductivity σ_s is inferred from this, to be $8.7 \times 10^{-9}\ \Omega^{-1}$, three orders of magnitude smaller than the one found by Hasegawa *et al* for the same system [77].

The use of this technique entails a number of potential problems and pitfalls. First of all, it has to be clear that the insulating trench is indeed insulating. This can be (and has been) verified by taking tunnelling spectra in the region of the trench [78]. Another point which needs further clarification is the role of the tunnelling voltage. In a genuine transport experiment, only the electrons at the Fermi surface are of any relevance. Here, tunnelling proceeds into (and out of) a wide energy range. Strictly speaking, it would be appropriate to infer the surface conductivity from data taken at very small tunnelling voltage only. To the best of our knowledge, the

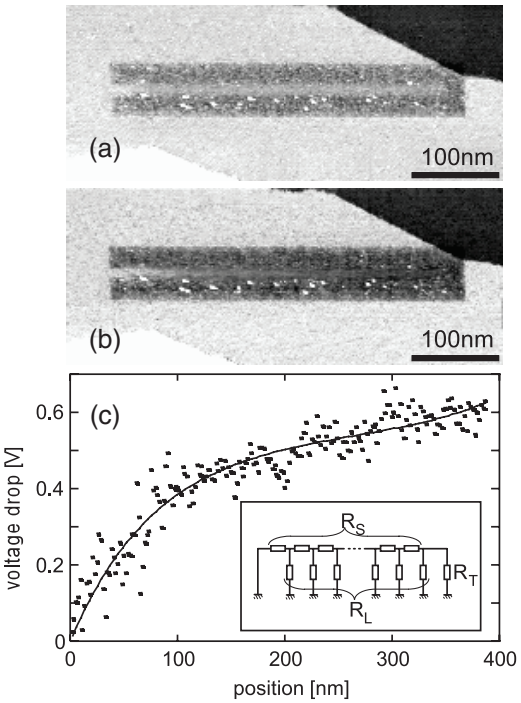

Figure 3. Results from Heike *et al* [78]: filled and empty STM images of an artificially fabricated tongue structure observed at tunnelling voltages of (a) −2.0 V and (b) +2.0 V. (c) Voltage drop along the structure for positive-bias observation. The solid line is a calculated curve fitted to the experimental data using the electrical circuit model shown in the inset.

dependence of the resulting surface sheet conductivity on the tunnelling parameters has not been tested systematically.

In principle, it should be possible to use an alternative STM approach in which a macroscopic current is passed through the sample and the potential at the surface is mapped. In this way, one performs a three-contact measurement in which one contact (the STM tip) is free to move across the surface. One should thus be able to mimic a four-point probe measurement with all its advantages by mapping the potential at different points. A technical problem in this approach is that the scanning range of an STM is usually very small and so will be the potential change between different points on a surface.

A promising approach to resolve some of the issues associated with using an STM in a one-contact surface conductance measurement is atomic force microscopy (AFM) with a conductive tip [79, 80]. The key idea of this technique is that the force/structural measurement is separated from the electrical measurement and the difficulty of a vacuum gap between the tip and the sample is avoided. This technique is particularly appropriate for measuring the conductance through adsorbed molecules on a surface but it has also been employed to study the local conductance of semiconductor heterostructures [80, 81].

3.2. Small-scale four-point probes

As discussed above, one of the fundamental problems with two-contact measurements is the unavoidable and unknown contribution of the contact resistance. This is especially problematic for very good conductors (because the contact resistance dominates the measurements), for semiconducting samples (because of the Schottky barrier), and for small probes (because of their high absolute resistance). The solution to this problem has been known and used for many years [82], and is prized for its simplicity: by using four contacts instead of two, one can measure the potential drop across contacts which do not carry a current. In this way, it is simple to show that the measured resistance is independent of the contact resistance—no matter whether the contacts are ohmic or not. In the following, we first focus on collinear four-point probes with equi-distant contact spacing, as depicted in figure 2. An alternative four-point geometry frequently used for macroscopic measurements is a square arrangement as suggested by van der Pauw [83].

While the four-contact approach solves the problem of large and non-ohmic contact resistance, the fundamental issue of surface sensitivity remains. It turns out that surface sensitivity can be achieved by using very small contact distances. To see this, consider how the measured four-point probe resistance R^{4pp} depends on the contact spacing. R^{4pp} is *defined* as the voltage drop U over the inner two contacts of the four-point probe divided by the current I passed through the outer contacts.

Expressions for the four-point probe resistance can be developed along the same lines as for the two-point probe resistance (see [82, 84, 85]). For an infinite 2D conductor with uniform sheet conductivity σ_s one finds

$$R^{4pp}_{2D} = \frac{1}{\pi\sigma_s}\ln\left(\frac{2s-r}{s+r}\right) \tag{4}$$

and for the semi-infinite bulk one obtains [84]

$$R^{4pp}_{3D} = \frac{1}{\pi\sigma_b}\left(\frac{1}{s+r}-\frac{1}{2s-r}\right). \tag{5}$$

Again, s is the spacing between adjacent point contacts and r their radius [84].

In contrast to the two-contact solution, it is also possible to determine the four-contact resistance in the case of point contacts, resulting in

$$R^{4pp}_{2D} = \frac{U}{I} = \frac{\ln 2}{\pi\sigma_s}, \tag{6}$$

and

$$R^{4pp}_{3D} = \frac{U}{I} = \frac{1}{2\pi s\sigma_b}, \tag{7}$$

for the 2D and 3D cases, respectively.

This is an important difference between a two-contact and a four-contact measurement. The latter is not only favourable because of the irrelevance of the contact resistance but also because no assumptions about the contact shape and size are required, if only they are small enough. Qualitatively, it is easy to understand why this is so. The electrostatic potential changes very rapidly in the vicinity of the current sources and slowly in between them. In a four-point measurement the voltage measuring probes are placed between the current

sources and their size and position is therefore not very critical. In a two-point measurement, on the other hand, the contacts act simultaneously as current sources and voltage probes and their geometry is therefore an important factor. To the best of our knowledge, the analytical result for the contact size dependence in equations (2)–(5) has not yet been tested experimentally.

The path to a surface-sensitive measurement is evident from comparing (6) and (7). The measured resistance in a 2D case (6) does not depend on the probe spacing, but that for the 3D case (7) gives rise to a higher four-point probe resistance for a smaller probe spacing. If we still regard the sample as two parallel resistors (representing the surface and the bulk), surface-sensitive measurements can be performed for values of s which are so small that the current transport proceeds entirely through the surface.

Equations (4)–(7) apply only to the collinear four-point probe with an equi-distant contact spacing, as shown in figure 2, but similar arguments can be made for other probe configurations, such as collinear four-point probes with variable probe spacings [86] or probes using the van der Pauw geometry [83]. The relations for the latter are particularly similar to (6) and (7) in that they only differ by the numerical constants.

The inverse dependence of R_{3D}^{4pp} on s is rather counter-intuitive. Qualitatively, it can be understood by inspecting the simple sketch in figure 4. Consider the case of a 2D conducting sheet, as shown in figures 4(a) and (b). If the distance between the current carrying contacts is very small, the current proceeds through the sheet without much spread. When the distance is increased, the current has to go a longer way but at the same time it can spread out on the sheet in the direction perpendicular to the probe. The reduction in resistance caused by this spreading of the current compensates the resistance increase due to the longer distance exactly, and the resulting four-point resistance is independent of the probe spacing. The situation for a semi-infinite 3D conductor is shown in figures 4(c) and (d). Again, the current spreads out perpendicular to the probe direction when the distance between the contacts is increased. In this case, however, the current can also spread into the sample, which leads to an over-compensation of the resistance increase caused by the longer distance, and thus to a lowering of the measured four-point probe resistance.

While the small scale turns a four-point probe surface sensitive, it also brings about problems which do not exist for macroscopic four-point probes. Whilst the measured resistance is independent of the contact resistance, the contact resistances are still able to manifest themselves in other ways. The connecting wires may have a small, but not insignificant, capacitance. This, together with the sometimes very large contact and wire resistance, results in a significant time constant, thus making fast AC measurements not easily achievable.

Different designs have been proposed for surface-sensitive four-point measurements. The most straightforward approach is viable in the case of a highly conductive surface on a poorly conducting bulk because the probe does not have to be particularly small. Measurements with macroscopic contacts, pre-fabricated on the macroscopic samples, were pioneered by the group of Henzler [87–89]. Despite their reduced flexibility compared to the approaches listed in the following, they are still an important method, in particular because of their high stability when temperature-dependent data is to be collected [90, 91].

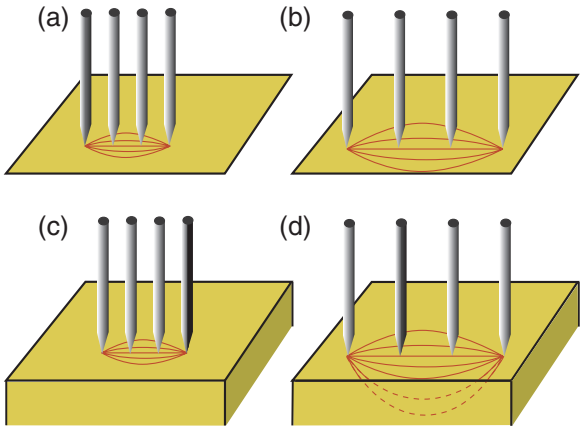

Figure 4. Qualitative illustration of the current's path for a variable-spacing four-point probe on a 2D ((a) and (b)) and semi-infinite 3D conductor ((c) and (d)).

The diametrical approach in many ways is the use of four independently driven STM tips (4-STM in the following), pioneered by the group of Hasegawa [92–95]. This offers ultimate flexibility and smallness. A particularly intriguing feature of the 4-STM approach is the possibility to combine conductance measurements with atomic resolution microscopy and/or to direct the tips of the STMs to microscopic objects with the help of a scanning electron microscope (SEM). Figure 5 illustrates some recent progress in this field. Figures 5(a) and (b) demonstrate a 4-STM which is simultaneously capable of taking temperature-dependent conductance measurements and atomic resolution images. Figure 5(c) shows a further step towards smaller probes, which is achieved by fabricating the contacts from carbon nanotubes coated with a metal. In this way, very small contact spacings and contact areas can be achieved.

An instructive result of the 4-STM approach is figure 6, which shows the measured four-point probe room temperature resistance of a clean Si wafer, i.e. with a Si(111)(7 × 7) surface, and of a wafer with the $(\sqrt{3} \times \sqrt{3})$Ag–Si(111) structure prepared on one face, as the probe spacing is varied over three orders of magnitude [92, 96]. In this particular experiment, the 4-STM is operated as a linear and equi-distant four-point probe, even though it is not restricted to do so. The light blue area in the figure symbolizes the four-point probe resistance which would be expect for a semi-infinite crystal with the bulk properties of the wafer in question, showing the power-law behaviour expected from (7). The data for the clean surface follow this expected behaviour but only for intermediate probe spacings. For a very large spacing the measured resistance is higher than the expected value because the current cannot spread out due to the finite thickness of the

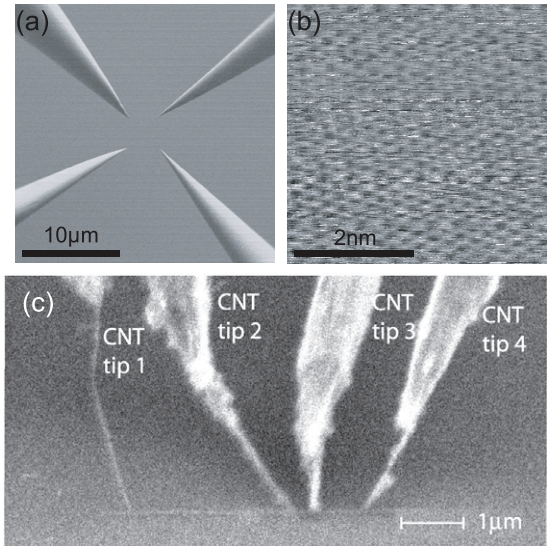

Figure 5. (a) SEM image of four tungsten tips arranged in a square of about 5 μm side length. (b) STM image of highly oriented pyrolytic graphite taken with one of the four tips. The tip bias is 0.2 V with tip current of 1.0 nA (reproduced with permission from [94]. Copyright 2007, American Institute of Physics). (c) SEM image of a $CoSi_2$ nanowire being contacted with four PtIr-coated carbon nanotube tips (reproduced with permission from [95]. Copyright 2007 American Chemical Society).

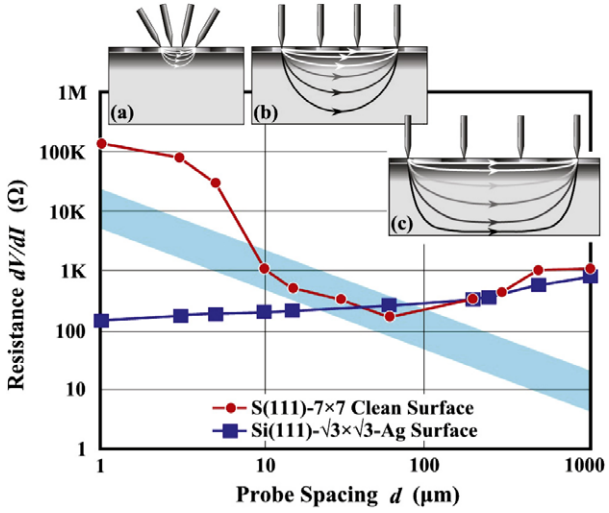

Figure 6. Electrical resistance of a silicon wafer, measured as a function of probe spacing with a collinear four-point probe formed from a 4-STM. Red circles show the result for the clean Si(111)(7 × 7) surface and blue squares for $(\sqrt{3} \times \sqrt{3})$Ag–Si(111). The light blue bar represents the expected resistance for a bulk-sensitive measurement on a wafer with the doping of the sample. The insets (a)–(c) schematically show the current flow distribution in the sample for the case of different probe spacings for Si(111)(7 × 7) (reproduced from [92, 96] with permission. Copyright 2001 Elsevier and 2003 Wiley, respectively).

wafer, as symbolized in inset (c). As expected, this happens when the contact spacing is of the same order of magnitude as the wafer thickness. For a very small spacing the measured resistance is also higher than the expected value for the bulk, but this is related to the presence of the space-charge layer close to the surface, which, in this case, is a poorer conductor than the bulk.

The $(\sqrt{3} \times \sqrt{3})$Ag–Si(111) surface shows an entirely different behaviour. For this system the resistance is almost independent of the probe spacing, strongly reminiscent of the behaviour predicted for a 2D system according to (6). In a more in-depth discussion below, we shall indeed see that $(\sqrt{3} \times \sqrt{3})$Ag–Si(111) has a far higher surface conductivity than Si(111)(7 × 7), which can completely dominate the bulk conductivity in many situations, such as here for probe spacings smaller than 10 μm or so.

The only major drawback of the 4-STM solution is its complexity. A one-head STM is already a complex instrument, especially when temperature-dependent measurements are of interest. Having four STM heads adds considerably to the experimental difficulties. This may be the reason why not many results have been published using this technique, even though the proof of principle has been given. An additional difficulty is the need for a less compact design of the STM heads, such that four heads can be operated very close to each other. The use of long cantilevers to support the STM tips can in practice lead to poorer resolution.

An alternative approach for four-point measurements is that of monolithic microscopic four-point probes which are commercially available for use in air [97]. Images of such probes fabricated by CAPRES are shown in figure 7. Over the past few years, considerable progress has been made in terms of miniaturization and reliability of the probes. Figure 7(a) shows an early four-point probe with cantilevers fabricated of gold-coated SiO_2. An extension of the same principle is shown in figure 7(b). This 12-point probe allows a distance between the inner contacts of 1.5 μm. At the same time, having 12 contacts which can be used independently, opens the possibility for essentially variable contact distances, such that similar measurements to those shown in figure 6 can be performed. The overall geometry is, of course, always linear, a restriction which is not present for a 4-STM.

Figure 7(c) shows a fundamentally novel design of a monolithic four-point probe which is described in [98]. First of all, there is only one broad cantilever, which supports all the contacts. This gives a greatly improved stability to the probe. In particular, it is much better suited to deal with a misalignment between probe and sample. In the case of many individual cantilevers, such a misalignment often causes the outer contacts to be severely stressed or even to break before all of the remaining contacts are touching the sample. Having all the contacts on one cantilever also opens the path to further miniaturization. With this design a minimum spacing of the inner probes of 500 nm can be achieved routinely and 250 nm has been found to be the current limit of fabrication. Another fundamentally new feature is the coating material, which is TiW instead of Au. This is also of great practical importance, because it does not wear off easily when contact is made to the sample and it renders the probes CMOS compatible.

A clear advantage of the monolithic four-point probes is that they are relatively easy to use, especially when temperature-dependent measurements are required. The overwhelming majority of results in the field of surface

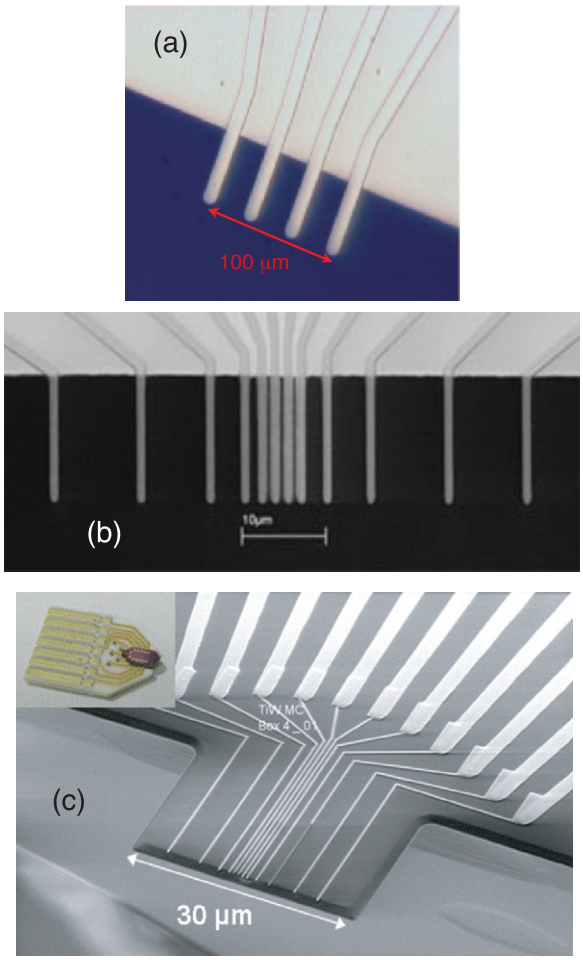

Figure 7. Monolithic four-point probes fabricated by CAPRES. (a), (b) Commercially available four- and 12-point probes which are fabricated from gold-coated SiO_2 cantilevers. (c) The novel development of a mono-cantilever probe, which supports TiW wires as contacts (reproduced with permission from [98]. Copyright 2008, American Institute of Physics). The inset in (c) shows such a probe mounted on a ceramic substrate.

conductivity has, indeed, been obtained with probes similar to those shown in figure 7(a). A possible drawback of having four (or more) physical contacts to the probe, as opposed to tunnelling contacts, is the risk of the contacts changing the properties of the sample in some way, for example through local stress resulting in surface deformation. There can be little doubt that the atomic and electronic structure of the surface is severely disturbed in the contact region. This should, in principle, not affect the measured conductance as long as the contact area is small compared to the distance between the contacts, an assumption made in the usual analysis of four-point data via (6) and (7). For the smallest possible monolithic four-point probes this assumption is not necessarily valid anymore and a 12-point probe, of which only four contacts are used, adds the potential problem of the other eight contacts influencing the measurement. So far, however, there is no experimental evidence suggesting that this is a problem, with different monolithic probes giving similar results for a quasi-two-dimensional electronic system (see the discussion of $(\sqrt{3} \times \sqrt{3})$Ag–Si(111) below). An important factor in understanding this is that the current in a four-point probe is not merely localized on a straight line between the contacts but spreads out considerably in the direction perpendicular to the probe axis (see figure 4 and [70, 85]), such that the effectively probed area is large compared to the contact area, even if the contacts are not point contacts and relatively close to each other.

3.3. Technical outlook

To summarize the technical situation for surface conductance measurements, several approaches are currently being pursued with different advantages and disadvantages. One-contact measurements with an STM are technically easiest but the interpretation of the data in terms of a surface conductivity is difficult. It is possible that some of the problems can be resolved by using conductive tip AFM instead of STM.

Two-contact STM measurements have not been tried in many cases but they are likely to suffer from similar interpretation problems as the one-contact measurements. A particular problem is that the character of the contact area appears to be crucial but is at the same time hard to assess. It is clearly too early to say if these challenges can be overcome [76]. However, two-contact measurements can be successfully applied to situations where one is primarily concerned by changes in conductivity, for example in magnetoresistive devices.

Four-contact STM is the most universal and versatile technique for surface-sensitive and nanoscale conductance measurements but it suffers from experimental complexity, especially when temperature-dependent measurements are of interest.

Monolithic four-point probes offer a technically unproblematic solution at the price of a fixed distance between the contacts. This problem can be partly overcome by having more than four contacts available on one probe. An important difference to the STM approaches is that a physical contact to the sample is needed, whereas a multi-tip STM can, in principle, work in a tunnelling regime, even though most experiments have also been carried out in contact with the sample.

Entirely contact-free measurements, optical, magnetic or otherwise, would be an interesting alternative. Optically induced currents and their decay have recently been studied for an unoccupied surface state [99], a measurement which effectively amounts to probing conductance, but not for the relevant states at the Fermi energy. There will probably be other reliable techniques to determine surface conductivity but it is hard to see how they can be made to work on a local level, for example in order to probe the conductivity of a nanoscale objects.

4. Case studies

In this section, we report results from a few systems for which the surface conductance has been studied. From what has been discussed above, it is clear that most of the cases refer to semiconductor surfaces, in this case the surfaces of Si, because surface sensitivity can only be achieved on the surface of a poor conductor. Historically, the most important test cases were the (7×7) reconstruction of Si(111) and the $(\sqrt{3}\times\sqrt{3})$Ag–Si(111)

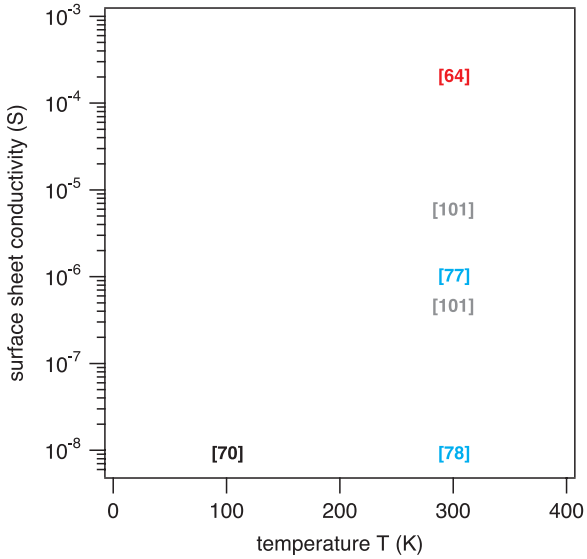

Figure 8. Two-dimensional conductivity of Si(111)(7 × 7) measured by different experimental techniques. The two data points from [101] correspond to wafers with different bulk doping, such that their difference in conductance must be due to bulk properties and not to surface conductivity. The experimental conductance from the original papers was converted into sheet conductivity when necessary, according to (6). Grey and black points refer to microscopic four-point probe data, red to a silicon-on-insulator sample and blue to single-tip STM.

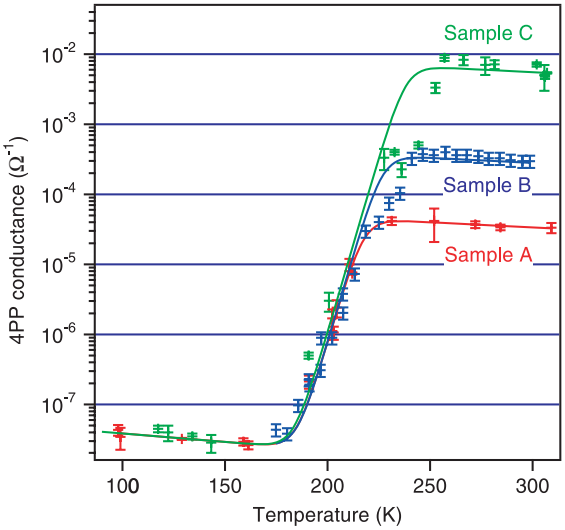

Figure 9. Temperature-dependent four-point probe conductance of Si(111)(7 × 7) for three samples with different levels of p doping. The contact separation is 10 μm. The solid lines are a guide to the eye. Adapted with permission from [70].

structure, which is formed when one monolayer of silver atoms is deposited on Si(111).

4.1. Si(111)(7 × 7)

The clean Si(111)(7 × 7) reconstruction is arguably the best known surface structure. The aspect of the geometrical structure, which had initially given rise to some debate, has been settled with general agreement on the model proposed by Takayanagi *et al* [100]. The character of the electronic structure, however, does not appear to be entirely settled (for recent references on this dispute, see [36, 39, 37]). In short, electron counting arguments would suggest the surface to be metallic. This is indeed supported by the most recent photoemission investigations [36, 37]. The electron density associated with the metallic state, on the other hand, is rather low and there is other experimental evidence which puts the surface close to a Mott–Hubbard insulating state [39]. In any case, even for the scenario of a metallic state, strong electron–phonon coupling appears to be present [37].

The experimental situation for surface conductance measurements on Si(111)(7 × 7) is summarized in figure 8. Not all available data points have been presented in the figure and the dependence on certain parameters such as bulk doping is not taken into account. The figure does not even show the full temperature dependence which has been reported for some cases [64, 101, 70]. Still, the presentation is useful to illustrate the great spread of the results and to discuss possible reasons for this.

The presentation of the figure acknowledges the possibility of a temperature-dependent surface conductivity, as appears likely in view of the strong electron–phonon coupling. It is important to note, however, that even strong electron–phonon coupling would only be expected to change the lifetime of the states by a factor of two or so over this temperature range. This is only a small change compared to the very wide spread of data points.

Indeed, the state of affairs appears to be dismal: even if we take into account only the points measured at room temperature, there is a spread of about five orders of magnitude. To make matters worse, it is not clear if the surface conductivity is 'metallic' in the sense of $\mathrm{d}\sigma/\mathrm{d}T < 0$ [64] or not [101]. Some experiments have even found it, unexpectedly, to depend on the bulk doping [101].

Much of this can be explained by referring back to the results of Shiraki *et al* [92], as shown in figure 6. It is immediately clear that four-point probe measurements on Si(111)(7 × 7) *at room temperature* need a probe spacing of much less than 10 μm in order to be surface sensitive. For probe spacings above this value, the measurement is primarily sensitive to only the bulk. At slightly smaller spacings the measurement would still be influenced mainly by the space-charge layer and surface sensitivity can only be expected at much smaller spacings. Note that the limit of 10 μm gives only the order of magnitude; the precise value depends strongly on the bulk doping.

Figure 9 also illustrates that a contact spacing of 10 μm is insufficient to achieve surface sensitivity at room temperature. The figure shows the temperature-dependent conductance of Si(111)(7 × 7) taken for three wafers with different levels of p doping using a four-point probe with 10 μm contact spacing [70]. The data measured at room temperature depend strongly on the bulk doping. Indeed, the measured value turns out to agree well with the semi-infinite three-dimensional model when using the bulk conductivity value supplied by the wafer manufacturer. At low temperature, however, the

results appear more likely to represent surface conductance because they are independent of the wafer doping. The transition between the two regimes happens because of the decreasing carrier concentration in the space-charge layer as the temperature is lowered. This will be explained below.

The fact that it is not possible to perform surface-sensitive measurements at room temperature using a microscopic four-point probe explains most of the data spread and the other peculiar findings associated with figure 8. Excluding the (grey) data points which suffer from this problem, only four values remain. Two of these agree rather well with each other, giving a conductivity of the order of 10^{-8} Ω^{-1}.

The data point with the highest reported sheet conductivity is from the work of Yoo and Weitering, who performed conductance measurements using a macroscopic van der Pauw probe based on ohmic contacts implanted into the sample [64]. The authors acknowledge the fact that such a geometry would inevitably lead to a conductance measurement dominated by the bulk and space-charge layer. Therefore, their measurements were not performed on a bulk Si wafer but on a so-called silicon on insulator sample, which consists of a very thin layer of silicon on a thick, insulating layer of silicon oxide. The thin silicon layer is assumed to be free of mobile carriers. It was, nevertheless, not possible to measure the clean surface conductance in this set-up. Therefore a difference technique was used in which the clean surface and an oxygen-covered surface were compared. This led to a small but clear difference, from which the data point in figure 8 was inferred as surface conductivity of the clean surface. This approach is not entirely without problems because it assumes that covering the surface with oxygen merely quenches the surface states without any other changes in the thin Si layer. If the surface conductivity is indeed as low as determined by some of the other approaches, it is conceivable that the observed differences are due to other factors.

A surface conductivity of 10^{-6} Ω^{-1} was obtained by Hasegawa *et al* using a single STM tip in contact with the sample [77]. For a detailed discussion of their approach see the previous section. While the influence of surface conductivity on their type of measurements is not exactly clear, it appears likely that there are other conductance channels in addition to the surface state conductance and that the reported value overestimates the true sheet conductivity.

The two remaining data points are the STM trench result from Heike *et al* discussed in the previous section [78] and the low temperature four-point probe result by Wells *et al* [70]. The data of the latter experiment have already been presented in figure 9 and the surface sheet conductivity presented in figure 8 can be directly read from the data points taken at the lowest temperature, assuming that they are dominated by the surface conductance. In the following we discuss why this assumption is indeed justified.

As already mentioned, the space-charge layer with its depth-dependent carrier concentration and conductivity calls for a more complex picture than that of a 2D sheet of conducting surface states on top of a isotropic 3D semi-infinite bulk; i.e., (6) and (7) cannot be used for an interpretation of data as shown in figure 9. Rigid attempts to take the space charge layer into account were laid out by Yoo and Weitering [64] and by Wells *et al* [70, 85]. The conductance in the space-charge layer has to be calculated in several steps [64]. The first is the determination of the band bending near the surface, as shown in figure 1. It depends entirely on the (temperature-dependent) position of the bulk Fermi level and the surface Fermi level pinning, which can be determined precisely by photoemission from core levels [102]. From the band bending, it is straightforward to determine the carrier concentration as a function of depth and temperature. From this, the depth and temperature-dependent conductivity can be calculated if the value for the carrier mobility is known; usually the bulk mobility is used. The expected sum of bulk and space-charge conductance can then be calculated from a finite-element solution of the Poisson equation [70, 85]. This forms the basis for the interpretation of figure 9.

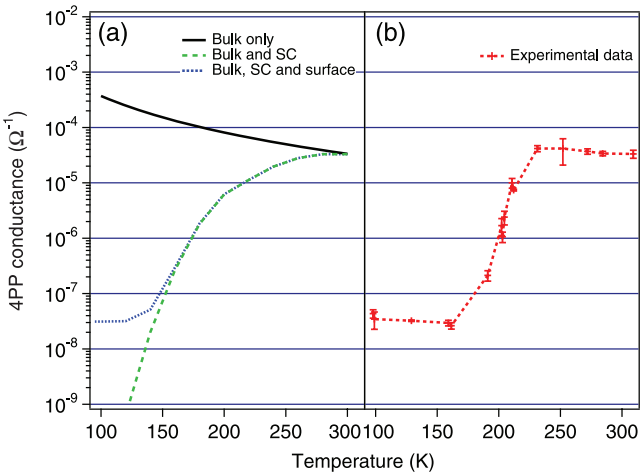

Figure 10. (a) Calculated four-point probe conductance for Si(111)(7 × 7) from a finite-element model for the bulk only, the bulk and space-charge (SC) layer combined and the bulk, SC layer and surface combined. (b) The experimental results, measured using a micro four-point probe taken from [70].

The result of such a calculation is shown in figure 10(a) and compared to the data for the correspondingly doped wafer in figure 10(b) [70]. The black line shows the expected conductance for only the semi-infinite bulk, which is terminated by flat bands without any space-charge layer. Interestingly, the calculated four-point conductance increases for lower temperatures in this case. This is somewhat counter-intuitive for a semiconducting bulk, for which it is frequently assumed that the number of bulk carriers increases strongly with temperature. For a doped semiconductor, however, the behaviour is not unusual. For the temperature interval of the calculation, the carrier concentration in the bulk is essentially constant since all the extrinsic carriers are excited across the gap but almost none of the intrinsic carriers are. Therefore, the temperature dependence of the bulk conductivity is dominated by the carrier mobility, and thus the bulk conductivity exhibits the same temperature dependence as that of a typical metal.

The dashed green line is the result of the finite-element calculation for the bulk with the space-charge layer present. At high temperature, there is good agreement between this

model and the data in figure 10(b), which is merely re-stating the fact that the measurements are bulk sensitive for these parameters. The model also correctly reproduces the drop at lower temperatures, which is due to a strong carrier depletion in the space-charge layer. The transition between these two regimes is somewhat steeper in the measurements than in the model, and this is attributed to the simplifications made in estimating the space-charge layer conductance.

At low temperatures, however, the agreement between the model and the data is poor. Below 160 K or so, the measured conductance is far higher than the expected value and this is attributed to the conduction through electronic surface states, which are not included in the model of the bulk and space-charge layer. At around 100 K, the expected conductance contribution of the bulk and space-charge layer is so small that the measured value was assigned to conduction through the surface layer only. When the measured surface conductance is included in the finite-element model, the dashed blue curve results, which agrees rather well with the experimental data in figure 10(b).

This rather complex argument justifies the interpretation of the low temperature conductance as caused by electronic surface states only. The resulting value of the surface sheet conductivity agrees very well with the room temperature STM result by Heike *et al*. Given that some doubts exist on the validity of the other data points in figure 8, it appears that the surface state conductivity of Si(111)(7 × 7) does indeed have such a low value. This would also explain the problems of measuring it: first because a leak current of any sort would give an artificially high value for the conductance; also, such a high resistance typically gives rise to a large time constant, thus there is a need to perform the measurements sufficiently slowly, and finally because of the small currents required.

Coming back to the initial discussion of the electronic structure of Si(111)(7 × 7), we can compare this measured value with the minimum for 2D metallic sheet conductivity according to the Ioffe–Regel criterion (which is $3.83 \times 10^{-5}\ \Omega^{-1}$ [64]). According to this comparison, the surface is clearly not in the metallic range. This finding appears consistent with a recent temperature-dependent and surface-sensitive NMR study of Si(111)(7 × 7), which suggests that the surface is close to a Mott–Hubbard-type metal–insulator transition [39]. It appears unlikely that the observed strong electron–phonon coupling [37] is sufficient to explain the low conductivity.

4.2. $(\sqrt{3} \times \sqrt{3})$Ag–Si(111)

Historically, the most important test system for direct surface conductance measurements has arguably been the $(\sqrt{3} \times \sqrt{3})$Ag–Si(111) structure. Many of the pioneering studies of the field by the groups of Henzler and Hasegawa were carried out on this surface. The most important advantage of $(\sqrt{3} \times \sqrt{3})$Ag–Si(111) over Si(111)(7 × 7) is the much higher surface sheet conductivity. There appears to be general agreement that, given an appropriate doping level, the surface conductance can be made higher than the conductance through the space-charge layer and the bulk, at least at room temperature. This makes the system an ideal test case for studying more subtle effects, such as additional doping of the Ag layer or the effect of steps.

The geometric and electronic structures of $(\sqrt{3} \times \sqrt{3})$Ag–Si(111) have been studied extensively. The structure is formed by exactly one monolayer (ML) of Ag atoms on Si(111), i.e. one Ag atom per surface atom of the unreconstructed surface. The geometric structure of the surface was long believed to be the so-called honeycomb-chained triangle (HCT) [103], but later the so-called inequivalent triangle (IET) model was found to have a lower total energy [104], and this was also confirmed experimentally [105, 106]. A puzzling fact remained: that the room temperature empty state STM images still resembled the more symmetric HCT model [107] while the low temperature (62 and 6 K) images were consistent with the IET model [108]. This apparent contradiction is widely thought to be caused by thermal fluctuations: at high temperature a rapid switching between the two possible domains in the IET model can be expected to generate averaged and HCT-like STM images while a fast technique, such as photoemission, still observes the characteristic features of the IET structure [109]. At low temperature, the fluctuations are frozen in and therefore STM shows a structure consistent with the IET model. However, the dispute over the nature and driving force of this phase transition is not settled. While many people favour the type of order–disorder transition mentioned above, others believe the transition to be of displacive character [106]. Very recently STM results reported the observation of the IET structure at room temperature, questioning the existence of the phase transition altogether [110].

The electronic structure of $(\sqrt{3} \times \sqrt{3})$Ag–Si(111) near the Fermi level is dominated by a free-electron-like surface state. This state is very sensitive to surface preparation. For the surface with exactly one monolayer Ag coverage, the bottom of the surface state band is located at the Fermi level. The state is thus unoccupied at zero temperature. At finite temperature it is occupied by thermally excited electrons. Electron doping of the surface, for example by a small excess Ag coverage, shifts the surface Fermi energy upwards, such that the number of free carriers on the surface is strongly enhanced [109, 63].

Characteristic features in the surface electronic structure have been used to study the character (and existence) of the aforementioned HCT–IET structure. From simple symmetry arguments it can be concluded that the transition from the HCT structure to the IET structure should lift the degeneracy of surface states bands at the $\bar{\mathrm{K}}$ point of the surface Brillouin zone. The bands in question are very close to each other and no conclusion could be reached on whether a lifting of the degeneracy between them can be observed or not [111, 112, 105, 113]. Moreover, recent theoretical evidence suggests that the splitting could be very small and therefore not detectable [114].

For the present purpose of conductance measurements, we can assume that the free-electron-like surface state is dominating the observed conductance, even though, for exactly one monolayer Ag coverage, the state is only thermally occupied. The observed surface conductance should be sensitive to contaminations, in particular excess Ag on the

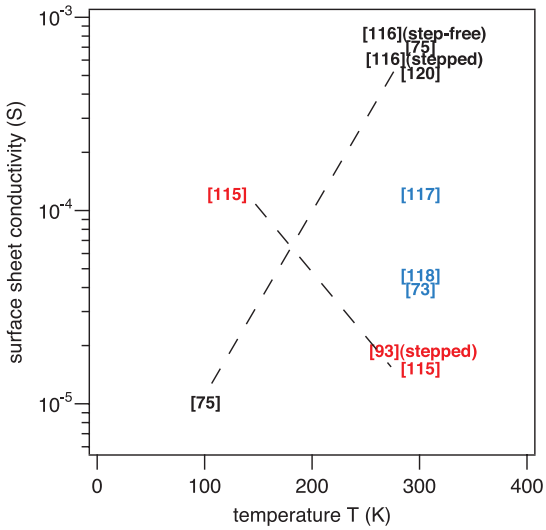

Figure 11. Two-dimensional sheet conductivity of $(\sqrt{3} \times \sqrt{3})$Ag–Si(111) from different experiments. The results from [115] and [75] represent the lowest and highest temperature of a complete temperature series. The dashed lines connecting these points are merely a guide to the eye, not the actual temperature dependence, which is given in figure 12. The low temperature data point from [75] could merely represent the bulk conductivity of the wafer. The data from [115] were taken from figure 2(c) in that paper. The data points for the almost step-free surface and for the stepped surface of [116] was taken from figure 4 in that paper. The value for a stepped surface from [93] was determined from the average of the reported sheet conductivities in the direction parallel and perpendicular to the step, an approach which is not strictly correct but sufficiently good to obtain an order of magnitude estimate. The value from [117] was taken from figure 3 in that paper. Black data points correspond to microscopic four-point probe results, blue data points to macroscopic four-point probes and red points to 4-STM. As in figure 8, experimental conductance from the original papers was converted into sheet conductivity when necessary according to (6).

surface. It is not clear if a surface phase transition is present, but if it is, one might expect it to show up in the temperature-dependent surface sheet conductivity.

Figure 11 shows the experimental results for the sheet conductivity. As in the case of Si(111)(7 × 7), a figure like this can only give an overview. The detailed temperature dependence which has been reported by some groups for this system [75, 115], is not included.

We first focus on the results obtained at room temperature. On the whole, the data spread is much smaller than for Si(111)(7 × 7). This is consistent with the generally agreed picture for the two surfaces: Si(111)(7 × 7) may be metallic or non-metallic but it is surely not expected to show a high surface conductivity. We have argued above that the true conductivity is very low indeed, and it is therefore not surprising that conduction through other channels could be mistaken for surface conductance. $(\sqrt{3} \times \sqrt{3})$Ag–Si(111), in contrast, is expected to have a high surface conductivity, which is relatively easy to measure. Qualitatively, this is confirmed by the fact that it has been possible to measure the surface conductance using macroscopic probes [118, 89, 119].

While much smaller than for Si(111)(7 × 7), the data spread at room temperature is still considerable and needs to be explained. Two possible sources of systematic error seem to be relevant. The most important one is probably surface imperfections such as monatomic steps, which are an almost unavoidable part of semiconductor surfaces. Again, $(\sqrt{3} \times \sqrt{3})$Ag–Si(111) is quite different from Si(111)(7 × 7) in this respect. For the latter, steps appear to have only a small effect, which is to increase the conductivity [85], whereas different studies on $(\sqrt{3} \times \sqrt{3})$Ag–Si(111) have shown that steps lead to a substantial decrease in conductivity [116, 93]. With this in mind, it appears reasonable to identify the data points at the top of the conductivity range as the intrinsic surface sheet conductivity of $(\sqrt{3} \times \sqrt{3})$Ag–Si(111). This appears to be confirmed by the data for which the step influence has actually been controlled. In [116] virtually step-free regions have been prepared by step-bunching and the position of the four-point probe on such a region has been controlled by electron microscopy. High conductivity is also observed for the smallest four-point probe, with a pitch of only 500 nm [120].

Another possible source of systematic error is unintentional electron doping into the surface state band because of an excess dosage of Ag on the surface. It has been shown by photoemission that even a small surplus coverage over the one monolayer required to form the $(\sqrt{3} \times \sqrt{3})$Ag–Si(111) can lead to a filling of the otherwise unoccupied surface state band. One can expect this to be reflected in an increased surface conductivity and this has indeed been observed in several experiments [118, 117, 73, 87]. However, the effect is not especially big. In all works except the (low temperature) result of Schad *et al*, the conductance change for going from 1 to 1.5 ML is less than a factor of two or so. Nakajima *et al* have also shown that the conductance change induced can also be time dependent [73]. The doping effect is reduced after a few hundred seconds because Ag atoms coalesce into islands, but only if the excess coverage exceeds a critical value (0.03 ML) for the nucleation of such islands.

Summarizing the room temperature results, most experiments agree on a sheet conductivity of the order of $5 \times 10^{-4}\ \Omega^{-1}$–$10^{-3}\ \Omega^{-3}$. There is some evidence to suggest that the higher values correspond to the perfect surface and a reduction in conductivity is observed in the case of steps being present. Interestingly, the two data points reporting the lowest sheet conductivity have been obtained by the 4-STM technique [93, 115]. It is rather puzzling that this should be so, because 4-STM is the technique which should offer the best control over the presence of steps on surfaces.

Unfortunately, the situation is much less clear for the low temperature conductivity. Complete temperature-dependent series have been reported by Wells *et al* [75] and Matsuda *et al* [115]. Both the data sets and the interpretation of these works are very different. The results are compared in figure 12.

As mentioned above, Matsuda *et al* find a very low value for the room temperature conductivity of a monolayer film, lower than any other value reported previously. Indeed, the room temperature value for one monolayer of Ag is even lower than that for 1.5 monolayers reported in the same paper, in contrast to all previous findings for the coverage dependence in this system [118, 117, 73, 87]. For a monolayer coverage, a strong increase in conductivity is found as the temperature

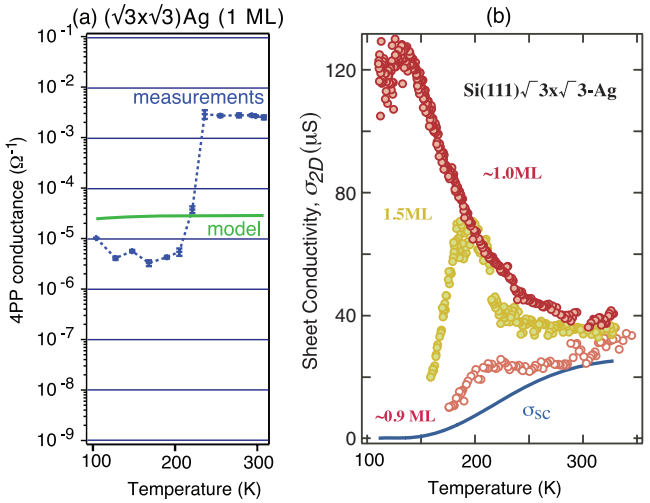

Figure 12. Temperature-dependent conductance for Ag-Si(111) from (a) [75] (reproduced with permission. Copyright 2007 IOP Publishing) and (b) [115] (reproduced with permission. Copyright 2007 by the American Physical Society). One ML corresponds to the $(\sqrt{3} \times \sqrt{3})$Ag–Si(111) structure. The green line in (a) and the blue line in (b) represent the expected conductivity for just the bulk and the space-charge layer.

is lowered. This is interpreted in terms of electron–phonon coupling. Interestingly, coverages different from exactly one monolayer show a very different behaviour, with a sharp transition to lower conductivity below 200 K (see figure 12).

In contrast to this, Wells *et al* find a high room temperature conductivity and a sharp transition to a lower conductivity at around 220 K. This transition was interpreted in terms of the HCT to IET phase transition. A simulation of the space-charge layer contribution to the measured conductance showed that the measured value was higher than the space-charge layer conductance for all temperatures investigated, which led the authors to conclude that the measured conductance is always related to surface states. Unfortunately, the calculated space-charge layer conductance at low temperatures turned out to be erroneously low [75]. A corrected calculation (as shown in figure 12) showed that the lower conductance at low temperature could indeed be due to the space-charge layer only. This error does not, however, affect the conclusion that the HCT to IET phase transition could be responsible for the sudden drop in conductivity at ≈220 K.

When comparing the data of Matsuda *et al* [115] and Wells *et al* [75], one notices that strong changes in the conductivity below room temperature have been found in both works. Wells *et al* report such a change for a complete monolayer whereas Matsuda *et al* find it for coverages below and above one monolayer, but not for exactly one monolayer. A possible way to reconcile the experimental results to some degree is therefore to assume an incorrect coverage in one of the works. But this is not really sufficient to reach agreement and one is forced to conclude that the temperature dependence of the surface sheet conductivity is not understood at present.

Matsuda *et al* have interpreted the drop in conductivity at low temperature for the off-monolayer coverage as a localization phenomenon caused by random potential modulations and defects, similar to localization in random systems. This interpretation is quite different from that given by Wells *et al*, who assign the transition to the HCT–IET surface phase transition. Another possible explanation for a steep drop in conductivity at low temperatures, which has not been given by either group, is the thermal emptying of the surface state band. For the ideal monolayer coverage of Ag, the surface state band at the $\bar{\Gamma}$ point is only thermally occupied. At lower temperatures, the narrowing of the Fermi–Dirac distribution will lead to a strong decrease in the number of mobile carriers, which should be reflected in the surface sheet conductivity.

We conclude the discussion of this system with another look at the properties of the space-charge layer. As mentioned above, the surface sheet conductivity of $(\sqrt{3} \times \sqrt{3})$Ag–Si(111) is rather high. In many situations the contribution of the space-charge layer is insignificant but this depends on the doping and the temperature and it can still be necessary to take the space-charge layer into account, as shown in figure 12. In the case of the wafer used by Matsuda *et al* [115] (n-doped 2–15 Ω cm) the space-charge layer still contributes noticeably to the room temperature conductance and this contribution has been subtracted by Matsuda *et al* [115] in order to obtain the data point reported in figure 11. For the wafer used by Wells *et al* [75] (p-doped, 190 Ω cm), on the other hand, the expected conductance of bulk and space-charge layer is insignificantly small at room temperature and the measured conductance is purely caused by the sheet conductivity of the surface states.

4.3. Other systems

The surface sheet conductivity of several other systems has been studied with microscopic probes. In particular, we draw attention to (5 × 2)Au-Si(111) [121, 122], $(\sqrt{21} \times \sqrt{21})$(Ag, Au)-Si(111) [123], Au–Si(557) [124], Au–Si(553) [125], the oxidation of Si surfaces [126], $(\sqrt{3} \times \sqrt{3})$Pb–Si(111) [127–129], the order to disorder transition on Si(001) [69], $CoSi_2$ nanowires [95], carbon nanotubes [130] and graphene [131, 132], which will not be discussed further here. Other systems, which are discussed in more detail below, are indium chains on Si(111) [133–135], Pb–Si(557) [90, 91], and the surface conductivity of Bi(111) [86, 136].

In the following, we choose to discuss a few examples in more detail. The first is the conductivity change due to a phase transition in quasi-one-dimensional (1D) chain structures on Si. For this we discuss two different systems, indium chains on Si(111) and 1D structures formed by the adsorption of lead on stepped Si surfaces. The transport properties of 1D structures are of interest because of the increased correlation for low-dimensional systems, the possibility of Peierls distortions, charge density waves, Luttinger liquid behaviour and other phenomena [43–46]. The second example is the surface sheet conductivity of Bi(111), both as a single crystal and as thin films on Si(111). Bismuth is a semimetal with a very low density of states at the Fermi level and a high density of metallic surface states. Therefore, it represents an important test case as to whether surface conductance can be observed for (poor) metals.

Quasi-1D zigzag chain structures are formed when indium is adsorbed on Si(111) [137]. This structure was found to

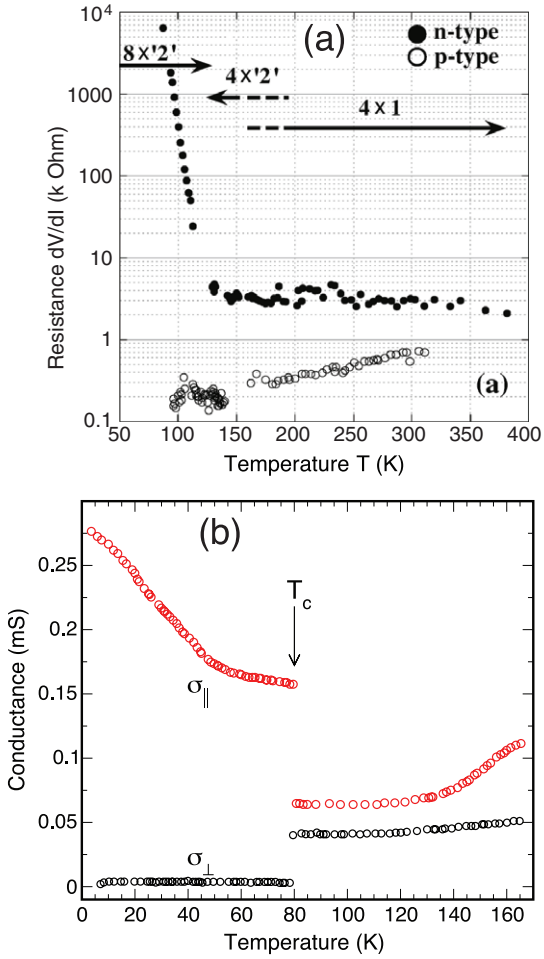

Figure 13. Conductance change associated with a surface phase transition. (a) In–Si(111) for both n- and p-doped substrates. Only the n-doped case permits surface-sensitive measurements and clearly shows a strong resistance change around 130 K (reproduced with permission from [135]. Copyright 2004 by the American Physical Society). (b) Anisotropic conductance change for Pb on Si(557) (reproduced with permission from [91]. Copyright 2007 Elsevier). Note that the switching for the two systems occurs in the opposite sense, i.e. the low temperature structure is more conductive for Pb on Si(557) and less conductive for In on Si(111).

undergo a metal–insulator phase transition when cooled below ≈130 K [138]. The detailed nature of the phase transition is still discussed, but a Peierls-type distortion appears to play a major role [138–146]. The four-point probe resistance of In–Si(111) is shown in figure 13(a). The temperature-dependent resistance was measured for the same structure prepared on p- and n-doped wafers [135]. In the p-doped case the resistance is much lower than in the n-doped case, and it was argued that this is because the space-charge layer dominates the transport. For the n-doped case the overall resistance is higher and a steep increase in the resistance was observed as the sample is cooled below ≈130 K. This was interpreted in terms of a surface sheet conductivity change.

The room temperature structure of In–Si(111) has a (4×1) periodicity. As the temperature is lowered, this is observed to turn into a (4 × '2') phase, with a periodicity doubling which is associated with the onset of the Peierls-type transition. However, this transition does not appear to affect the measured surface resistivity. This was ascribed to fluctuations in the Peierls phase which would still allow for conduction. A strong increase of the resistivity is observed at a second transition from (4 × '2') to (8 × '2') in which the reconstruction of neighbouring chains locks into phase.

This behaviour of a higher resistivity in the low temperature phase is certainly what is expected for a Peierls or charge density wave transition, even though the findings suggest that it is the 2D ordering, not the 1D ordering, which eventually gives rise to the conductivity change. It is intriguing that the *opposite conductivity change* is found for a seemingly similar system, Pb chains on Si(557).

Stepped Si surfaces such as Si(557) or Si(553) are excellent templates for growing highly periodic, one-dimensional structures by adsorbing metal atoms [42]. Pb on Si(557) is such a system, which can be prepared to give Pb chains with a regular inter-chain distance [90, 147, 91]. The temperature-dependent surface sheet conductivity of Pb on Si(557) was studied by Tegenkamp *et al* using four macroscopic contacts prepared on the surface of the sample. The probe geometry was designed such that the conductivity parallel and perpendicular to the chain direction could be measured. It was argued that the measured conductance was essentially due to the surface when the structure was prepared on a nominally undoped bulk [90, 91]. The measurements presented below confirm this inference. The reason for this is that Pb pins the surface Fermi level close to mid-gap, the band bending close to the surface is thus negligible and pure bulk behaviour would be expected in the absence of surface state conductivity. The measured conductance, however, was found to be considerably higher than the value expected for the semi-infinite bulk.

Figure 13(b) shows the result of the measurements. At high temperature (above 78 K) the surface conductivity is almost isotropic and it is consistent with a semiconducting electronic structure (i.e. $\mathrm{d}\sigma/\mathrm{d}T > 0$). Below 78 K the conductivity is highly anisotropic with a high, metallic (i.e. $\mathrm{d}\sigma/\mathrm{d}T < 0$) conductivity along the Pb chains and negligible surface conductivity perpendicular to the chains. As mentioned above, the conductivity change along the chains happens in the opposite direction as for In–Si(111) and as expected for a Peierls distortion in a 1D system.

The origin for this intriguing behaviour was recently discovered by angle-resolved photoemission [148]. The key to understanding the transition is, again, that the electronic structure is, in fact, not quasi-1D but truly 2D and that the arrangement of regular metallic chains below 78 K is related to the nesting of the 2D Fermi surface in the direction perpendicular to the chains.

The results of Tegenkamp *et al* also hold an interesting technical message. As we have seen earlier, the presence of the space-charge layer can be a major problem for surface transport measurements on semiconductors. The absolute number of carriers in the space-charge layer can be much higher than in the surface states and it depends on many parameters in a complex way. Ignoring the space-charge layer has been the origin of many incorrect results, even with microscopic four-point probes. The present case, on the other hand, illustrates

the advantages of a system for which the space-charge layer can be truly ignored. Most importantly, it is possible to use a macroscopic probe. The temperature can be varied over a wide range and essentially noise-free data are obtained.

It should also be noted that the results of figure 13(b) justify the assumption of a negligible bulk conductance because the phase transition is so remarkably sharp in temperature. We have seen in figure 9 that the mere switching from surface to bulk conduction could be mistaken for a phase transition, and several results which have been interpreted in terms of surface conductivity changes happen over a relatively large temperature interval and could possibly be misinterpretations, at least when the space-charge layer conductance is not carefully treated. Here, on the other hand, the transition is much too sharp to be related to a space-charge layer effect.

As a final example, we address the issue of measuring surface conductance on a (semi-) metal surface. When estimating the contact separation of a four-point probe which is needed to achieve surface sensitivity on a metal surface using (6) and (7), this appears to be an impossible task. The discussion here also falls short from addressing a highly conductive metal and rather focuses on the semimetal bismuth.

Bi has a very low density of states at the Fermi level, about five orders of magnitude lower than that of a typical metal such as copper [149]. This is to some degree compensated by the small effective mass of the carriers, resulting in a room temperature conductivity which is only two orders of magnitude smaller than that of a good conductor [150].

Another consequence of the small effective mass of the carriers combined with the small Fermi energy is a very long effective de Broglie wavelength and a high mobility. This leads to pronounced quantum size effects in thin Bi films [151]. Soon after the discovery of this phenomenon, it was argued that the overlap of valence and conduction bands should vanish altogether for films with a thickness of less than approximately 20–30 nm [152, 153], and the semimetal should hence turn into a semiconductor. More than 30 years after this prediction and after considerable experimental and theoretical effort (see for example [154–159] and references therein), it remains unclear if this transition takes place or not.

An important obstacle for observing the transition would be a surface state induced, metallic sheet conductivity which could inhibit the observation of a semiconducting film [154, 155, 157]. It was indeed found that many low-index surfaces of Bi studied are good two-dimensional metals [13, 12, 14, 160] (for a review see [15]), in the sense of supporting metallic surface states which increase the density of states at the Fermi level. The existence of the states was shown to be related to the symmetry breaking at the surface combined with the strong spin–orbit interaction in Bi [161, 162]. Ultra-thin, high quality films of epitaxial Bi(111) were found to have the same surface electronic structure as the bulk crystal, confirming the notion that they should play a role in the transport properties of the films [123, 163][3]. Given the possible importance of the metallic surface states for the conductivity of thin films, it would be interesting to know the sheet conductivity caused by them.

[3] Note that the previous reference uses a different notation for the orientation of the Bi film. What we refer to as Bi(111), using the rhombohedral crystal system, is referred to as Bi(001) by them, using a hexagonal description with one of the four indices omitted.

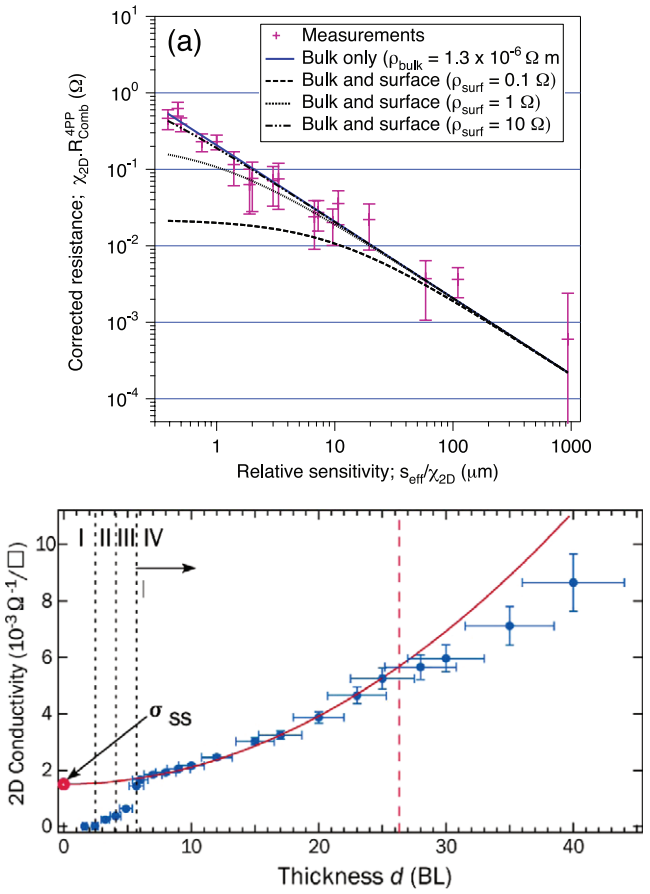

Figure 14. (a) Measured four-point resistance of a single crystal of Bi(111), corrected to incorporate the surface sensitivity ($\chi_{2D} R^{4pp}_{comb}$) and plotted against the relative (bulk) sensitivity s_{eff}/χ_{2D} (reproduced with permission from [86]. Copyright 2008 American Institute of Physics, which should also be considered for the definition of $\chi_{2D} R_{comb}$ and s_{eff}/χ_{2D}, which are closely related to the genuine four-point probe resistance and the contact spacing, respectively). The solid line indicates the expected behaviour for a bulk dominated measurement and the black dashed lines indicate the expected behaviour for the combined bulk and surface terms (using surface resistivities of 0.1, 1 and 10 Ω). (b) Sheet conductivity as a function of thickness (in bilayers) for a thin film of Bi(111) grown on Si(111). The solid line shows a parabolic fit for a thickness between 6 and 25 bilayers (reproduced with permission from [136]. Copyright 2007, American Institute of Physics).

Wells *et al* have tried to determine the sheet conductivity of the surface states on the (111) surface of a bismuth single crystal using a 12-point probe such that different contact spacings could be used [86]. The advantage of this approach is that the conductivity of the underlying bulk is well known, even though surface scattering might play a role. Their result is given in figure 14(a). Essentially, it shows the measured four-point probe resistance as a function of contact spacing together with calculations for the pure bulk behaviour as well as the behaviour for the bulk plus a surface with a certain sheet resistance. The measured data fit well with the bulk behaviour, and surfaces with low sheet resistance (0.1 or 1 Ω)

can definitely be excluded. A higher surface sheet resistance of 10 Ω or more would, however, be consistent with the data.

The measurements in figure 14(a) were not only taken using all of the possible equi-distant four-point configurations of a 12-point probe but also employing more exotic configurations, such as non-equidistant spacings or not using the outer probes as current sources. In this way, it can be shown that the surface or bulk sensitivity can be increased over a configuration with an equi-distant spacing of the same order of magnitude. The quantities which are displayed in figure 14(a) are therefore not strictly the resistance and the probe spacing. Instead, they have been defined such that all possible probe configurations can be displayed and compared to each other [86]. In this way, it was possible to vary the ratio of surface to bulk sensitivity over three orders of magnitude.

Hirahara *et al* used a different approach to establish the surface sheet conductivity of Bi(111). They have measured the conductance of an ultra-thin film of Bi(111) grown on Si(111) as a function of film thickness [136]. Their result is shown in figure 14(b), giving the inferred sheet conductivity as a function of film thickness measured in bismuth bilayers (BL). The very low thickness regime of the graph (marked I–III) should be ignored for the present purpose because the film structure is different and the surface is not (111) [164]. For higher coverages the sheet conductivity can be described by a parabolic fit. It was argued that this type of increase would be expected for a film for which both the carrier density and the mobility are proportional to the thickness [136] and extrapolating the curve to zero thickness would give the surface sheet conductivity. This approach could be criticized by arguing that the assumption for a linearly increasing carrier concentration is certainly not valid for thin bismuth films, given the pronounced quantum size effects. However, one also notices that the result does not at all depend on this. Merely assuming some smooth behaviour and extrapolating the curve to zero coverage would produce a similar result for the surface state sheet conductivity.

The resulting value of the sheet conductivity is $1.5 \times 10^{-3}\ \Omega^{-1}$, which is consistent with the lower limit for the sheet resistance obtained by Wells *et al* [86]. Note, however, that the surface sensitivity of Wells *et al* has not been sufficient to firmly establish a value surface sheet conductivity on bulk bismuth, even though the smallest probe spacing used in their work had a contact distance of only 500 nm. Even for bismuth, which is a relatively poor metal with a rather conductive surface, surface sensitivity could not be achieved on a bulk crystal.

5. Conclusions and outlook

Surface-sensitive conductance measurements are a relatively new and rapidly developing field. In this review, we have tried to illustrate the state of the art using a few examples, mainly focusing on the use of microscopic four-point probes but also discussing alternative approaches, some of which are still very much in the stage of development.

Using microscopic four-point probes, it is now possible to measure genuine surface sheet conductivity on many semiconductor surfaces. The bulk and the space-charge layer can give rise to serious difficulties because their conductance can be much higher than that of the clean surface. If the surface Fermi level and the bulk properties are known, however, it is always possible to calculate the space-charge layer contribution to the measured conductance. Surface-sensitive measurements on metal surfaces are not currently possible and it is hard to see that this situation can be improved upon in the very near future.

On the technical side, a trend to ever smaller probes can be foreseen because of the increased surface sensitivity and because of the possibility to measure the conductance of genuine nanostructures deposited or fabricated on a surface. For the latter, the combination of conductance measurements with a microscopic technique (STM or electron microscopy) is highly desirable. Other possible developments include non-contact techniques or conductance measurements using only one probe on a microscopic scale (such as one STM tip) while supplying the current macroscopically.

The few examples of scientific results given in this review represent the state of the field but fall short of the exploring the many possibly interesting systems mentioned in the introduction. Given the rapid technical improvements, more results for quantum size effects, adsorbates on surfaces, metal–insulator transitions etc can be expected for the near future.

Acknowledgments

The authors wish to acknowledge stimulating discussions with Peter Petersen, Mette Balslev and Jesper Hansen at CAPRES A/S, Torben Hansen, Peter Bøggild and Lauge Gammelgaard at the Technical University of Denmark, Bert Voigtländer and Philipp Jaschinsky at FZ-Jülich, Herbert Pfnür at the Universität Hannover and Shuji Hasegawa at the University of Tokyo. The latter two groups as well as Seiji Heike are also acknowledged for their kind permission to reproduce figures of their work in this review. The project for conductance measurements at the University of Aarhus was funded by the Danish Ministry of Science, Technology and Innovation through the MiNaP innovation consortium. PH thanks the Surface Science Research Centre at the University of Liverpool for their hospitality and the Leverhulme Foundation for supporting a stay there, during the period in which this review was written.

References

[1] Gartland P O and Slagsvold B J 1975 *Phys. Rev.* B **12** 4047–58
[2] Heimann P, Neddermeyer H and Roloff H F 1977 *J. Phys. C: Solid State Phys.* **10** L17–22
[3] Hansson G V and Flodström S A 1978 *Phys. Rev.* B **18** 1562–71
[4] Karlsson U O, Hansson G V, Persson P E S and Flodström S A 1982 *Phys. Rev.* B **26** 1852
[5] Levinson H J, Greuter F and Plummer E W 1983 *Phys. Rev.* B **27** 727–47
[6] Bartynski R A, Jensen E, Gustafsson T and Plummer E W 1985 *Phys. Rev.* B **32** 1921–6
[7] Plummer E W and Hannon J B 1994 *Prog. Surf. Sci.* **46** 149

[8] Matzdorf R 1998 *Surf. Sci. Rep.* **30** 153–206
[9] Reinert F, Nicolay G, Schmidt S, Ehm D and Hüfner S 2001 *Phys. Rev.* B **63** 115415
[10] Hofmann Ph, Søndergaard Ch, Agergaard S, Hoffmann S V, Gayone J E, Zampieri G, Lizzit S and Baraldi A 2002 *Phys. Rev.* B **66** 245422
[11] Kim T K, Sorensen T S, Wolfring E, Li H, Chulkov E V and Hofmann Ph 2005 *Phys. Rev.* B **72** 075422
[12] Ast Ch R and Höchst H 2001 *Phys. Rev. Lett.* **87** 177602
[13] Agergaard S, Søndergaard C, Li H, Nielsen M B, Hoffmann S V, Li Z and Hofmann Ph 2001 *New J. Phys.* **3** 15.1–15.10
[14] Hofmann Ph, Gayone J E, Bihlmayer G, Koroteev Yu M and Chulkov E V 2005 *Phys. Rev.* B **71** 195413
[15] Hofmann Ph 2006 *Prog. Surf. Sci.* **81** 191–245
[16] Sandl P and Bertel E 1994 *Surf. Sci.* **302** L325–30
[17] Eberhardt W, Greuter F and Plummer E W 1981 *Phys. Rev. Lett.* **46** 1085–8
[18] Greuter F, Heskett D, Plummer E W and Freund H J 1983 *Phys. Rev.* B **27** 7117–35
[19] Rotenberg E and Kevan S D 2002 *J. Electron Spectrosc. Relat. Phenom.* **126** 125
[20] Chiang T C 2000 *Surf. Sci. Rep.* **39** 181–235
[21] Milun M, Pervan P and Woodruff D P 2002 *Rep. Prog. Phys.* **65** 99–141
[22] Plummer E W and Dowben P A 1993 *Prog. Surf. Sci.* **42** 201–16
[23] Dowben P A 2000 *Surf. Sci. Rep.* **40** 151–245
[24] Tosatti E 1975 *Festkörperprobleme* **15** 113–47
[25] Mascaraque A and Michel E G 2002 *J. Phys.: Condens. Matter* **14** 6005–35
[26] Carpinelli J M, Weitering H H, Plummer E W and Stumpf R 1996 *Nature* **381** 398–400
[27] Carpinelli J M, Weitering H H, Bartkowiak M, Stumpf R and Plummer E W 1997 *Phys. Rev. Lett.* **79** 2859–62
[28] Cortes R, Tejeda A, Lobo J, Didiot C, Kierren B, Malterre D, Michel E G and Mascaraque A 2006 *Phys. Rev. Lett.* **96** 126103
[29] Profeta G and Tosatti E 2007 *Phys. Rev. Lett.* **98** 086401
[30] Modesti S, Petaccia L, Ceballos G, Vobornik I, Panaccione G, Rossi G, Ottaviano L, Larciprete R, Lizzit S and Goldoni A 2007 *Phys. Rev. Lett.* **98** 126401
[31] Johansson L I, Owman F and Martensson P 1996 *Surf. Sci.* **360** L478–82
[32] Themlin J M, Forbeaux I, Langlais V, Belkhir H and Debever J M 1997 *Europhys. Lett.* **39** 61–6
[33] Northrup J E and Neugebauer J 1998 *Phys. Rev.* B **57** R4230
[34] Ramachandran V and Feenstra R M 1999 *Phys. Rev. Lett.* **82** 1000–3
[35] Weitering H H, Shi X, Johnson P D, Chen J, DiNardo N J and Kempa K 1997 *Phys. Rev. Lett.* **78** 1331–4
[36] Losio R, Altmann K N and Himpsel F J 2000 *Phys. Rev.* B **61** 10845–53
[37] Barke I, Zheng F, Konicek A R, Hatch R C and Himpsel F J 2006 *Phys. Rev. Lett.* **96** 216801–4
[38] Demuth J E, Persson B N J and Schellsorokin A J 1983 *Phys. Rev. Lett.* **51** 2214–7
[39] Schillinger R, Bromberger C, Jansch H J, Kleine H, Kuhlert O, Weindel C and Fick D 2005 *Phys. Rev.* B **72** 115314
[40] Guo Y *et al* 2004 *Science* **306** 1915–7
[41] Himpsel F J, Kirakosian A, Crain J N, Lin J L and Petrovykh D Y 2001 *Solid State Commun.* **117** 149–57
[42] Barke I, Rugheimer T K, Zheng F and Himpsel F J 2007 *Appl. Surf. Sci.* **254** 4–11
[43] Gruner G 1988 *Rev. Mod. Phys.* **60** 1129–82
[44] Grüner G 1994 Density waves in solids *Frontiers in Physics* vol 89 (Cambridge, MA: Perseus Publishing)
[45] Thorne R E 1996 *Phys. Today* **42** (May) 42–7
[46] Voit J 1995 *Rep. Prog. Phys.* **58** 977–1116
[47] Crain J N, Kirakosian A, Altmann K N, Bromberger C, Erwin S C, McChesney J L, Lin J L and Himpsel F J 2003 *Phys. Rev. Lett.* **90** 176805–4
[48] Crain J N, McChesney J L, Zheng F, Gallagher M C, Snijders P C, Bissen M, Gundelach C, Erwin S C and Himpsel F J 2004 *Phys. Rev.* B **69** 125401
[49] Riikonen S and Sanchez-Portal D 2005 *Nanotechnology* **16** S218–23
[50] Snijders P C, Rogge S and Weitering H H 2006 *Phys. Rev. Lett.* **96** 076801
[51] Rosei F, Schunack M, Naitoh Y, Jiang P, Gourdon A, Laegsgaard E, Stensgaard I, Joachim Ch and Besenbacher F 2003 *Prog. Surf. Sci.* **71** 95
[52] Feyter S De and De Schryver F C 2003 *Chem. Soc. Rev.* **32** 139–50
[53] Papageorgiou N, Salomon E, Angot T, Layet J M, Giovanelli L and Lay G Le 2004 *Prog. Surf. Sci.* **77** 139–70
[54] Barth J V, Costantini G and Kern K 2005 *Nature* **437** 671–9
[55] Jung T A, Schlittler R R and Gimzewski J K 1997 *Nature* **386** 696–8
[56] Rosei F, Schunack M, Jiang P, Gourdon A, Lagsgaard E, Stensgaard I, Joachim C and Besenbacher F 2002 *Science* **296** 328–31
[57] Kuntze J, Berndt R, Jiang P, Tang H, Gourdon A and Joachim C 2002 *Phys. Rev.* B **65** 233405
[58] Wolkow R A 1999 *Annu. Rev. Phys. Chem.* **50** 413–41
[59] Upward M D, Beton P H and Moriarty P 1999 *Surf. Sci.* **441** 21–5
[60] Theobald J A, Oxtoby N S, Phillips M A, Champness N R and Beton P H 2003 *Nature* **424** 1029–31
[61] Gustafsson J B, Zhang H M, Moons E and Johansson L S O 2007 *Phys. Rev.* B **75** 155413
[62] Gustafsson J B, Zhang H M and Johansson L S O 2007 *Phys. Rev.* B **75** 155414
[63] Crain J N, Gallagher M C, McChesney J L, Bissen M and Himpsel F J 2005 *Phys. Rev.* B **72** 045312
[64] Yoo K and Weitering H H 2002 *Phys. Rev.* B **65** 115424
[65] Roll A and Motz H 1957 *Z. Metallk.* **48** 272–80
[66] Srivastava P L, Sinha S and Singh R N 1989 *J. Phys.: Condens. Matter* **1** 1695–705
[67] Kondo J 1964 *Prog. Theor. Phys.* **32** 37
[68] Lüth H 1992 *Surfaces and Interfaces of Solid Materials* 3rd edn (Berlin: Springer)
[69] Yoo K and Weitering H H 2001 *Phys. Rev. Lett.* **87** 026802
[70] Wells J W, Kallehauge J F, Hansen T M and Hofmann Ph 2006 *Phys. Rev. Lett.* **97** 206803
[71] Hollinger G and Himpsel F J 1983 *J. Vac. Sci. Technol.* A **1** 640–5
[72] Kono S, Higashiyama K, Kinoshita T, Miyahara T, Kato H, Ohsawa H, Enta Y, Maeda F and Yaegashi Y 1987 *Phys. Rev. Lett.* **58** 1555–8
[73] Nakajima Y, Takeda S, Nagao T and Hasegawa S 1997 *Phys. Rev.* B **56** 6782
[74] Crain J N, Altmann K N, Bromberger C and Himpsel F J 2002 *Phys. Rev.* B **66** 205302
[75] Wells J W, Kallehauge J F and Hofmann Ph 2007 *J. Phys.: Condens. Matter* **19** 176008
[76] Jaschinsky P, Wensorra J, Lepsa M I, Mysliveček J and Voigtländer B 2008 **20** at press
[77] Hasegawa Y, Lyo I-W and Avouris Ph 1996 *Surf. Sci.* **357/358** 32
[78] Heike S, Watanabe S, Wada Y and Hashizume T 1998 *Phys. Rev. Lett.* **81** 890–3
[79] Leatherman G, Durantini E N, Gust D, Moore T A, Moore A L, Stone S, Zhou Z, Rez P, Liu Y Z and Lindsay S M 1999 *J. Phys. Chem.* B **103** 4006–10
[80] Park J Y, Phaneuf R J, Ogletree D F and Salmeron M 2005 *Appl. Phys. Lett.* **86** 172105
[81] Park J Y, Qi Yabing, Ogletree D F, Thiel P A and Salmeron M 2007 *Phys. Rev.* B **76** 064108

[82] Smits F M 1958 *Bell Syst. Tech. J.* **37** 711–8
[83] van der Pauw L J 1958 *Philips Res. Rep.* **13** 1
[84] Jaschinsky P 2007 *PhD Thesis* RWTH Aachen
[85] Wells J W, Kallehauge J F and Hofmann Ph 2008 *Surf. Sci.* **602** 1742–9
[86] Wells J W, Handrup K, Kallehauge J F, Bøggild P, Balslev M B, Hansen J E, Petersen P R E and Hofmann Ph 2008 *J. Appl. Phys.* **104** 053717
[87] Schad R, Heun S, Heidenblut T and Henzler M 1992 *Phys. Rev.* B **45** 11430–2
[88] Schad R, Jentzsch F and Henzler M 1992 *J. Vac. Sci. Technol.* B **10** 1177–80
[89] Heun S, Bange J, Schad R and Henzler M 1993 *J. Phys.: Condens. Matter* **5** 2913–8
[90] Tegenkamp C, Kallassy Z, Pfnur H, Gunter H-L, Zielasek V and Henzler M 2005 *Phys. Rev. Lett.* **95** 176804
[91] Tegenkamp C and Pfnur H 2007 *Surf. Sci.* **601** 2641–6
[92] Shiraki I, Tanabe F, Hobara R, Nagao T and Hasegawa S 2001 *Surf. Sci.* **493** 633
[93] Matsuda I, Ueno M, Hirahara T, Hobara R, Morikawa H, Liu C and Hasegawa S 2004 *Phys. Rev. Lett.* **93** 236801
[94] Hobara R, Nagamura N, Hasegawa S, Matsuda I, Yamamoto Y, Miyatake Y and Nagamura T 2007 *Rev. Sci. Instrum.* **78** 053705
[95] Yoshimoto S *et al* 2007 *Nano Lett.* **7** 956–9
[96] Hasegawa S *et al* 2003 *Surf. Rev. Lett.* **10** 963–80
[97] www.capres.com
[98] Gammelgaard L, Boggild P, Wells J W, Handrup K, Hofmann Ph, Balslev M B, Hansen J E and Petersen P R E 2008 *Appl. Phys. Lett.* **93** 093104
[99] Gudde J, Rohleder M, Meier T, Koch S W and Hofer U 2007 *Science* **318** 1287–91
[100] Takayanagi K, Tanishiro Y, Takahashi S and Takahashi M 1985 *Surf. Sci.* **164** 367–92
[101] Tanikawa T, Yoo K, Matsuda I, Hasegawa S and Hasegawa Y 2003 *Phys. Rev.* B **68** 113303
[102] Himpsel F J, Hollinger G and Pollak R A 1983 *Phys. Rev.* B **28** 7014–8
[103] Takahashi T, Nakatani S, Okamoto N, Ishikawa T and Kikuta S 1988 *Japan. J. Appl. Phys.* 2 **27** 753–5
[104] Aizawa H, Tsukada M, Sato N and Hasegawa S 1999 *Surf. Sci.* **429** L509–14
[105] Matsuda I *et al* 2003 *Phys. Rev.* B **68** 085407
[106] Takahashi K, Tajiri H, Sumitani K, Akimoto K, Sugiyama H, Zhang X and Kawata H 2003 *Surf. Rev. Lett.* **10** 519–24
[107] Wan K J, Lin X F and Nogami J 1992 *Phys. Rev.* B **45** 9509–12
[108] Sato N, Takeda S, Nagao T and Hasegawa S 1999 *Phys. Rev.* B **59** 2035–9
[109] Matsuda I, Hirahara T, Konishi M, Liu C, Morikawa H, D'angelo M, Hasegawa S, Okuda T and Kinoshita T 2005 *Phys. Rev.* B **71** 235315
[110] Zhang H M, Gustafsson J B and Johansson L S O 2006 *Phys. Rev.* B **74** 201304
[111] Zhang H M, Sakamoto K and Uhrberg R I G 2001 *Phys. Rev.* B **64** 245421
[112] Uhrberg R I G, Zhang H M, Balasubramanian T, Landemark E and Yeom H W 2002 *Phys. Rev.* B **65** 081305
[113] Zhang H M and Uhrberg R I G 2006 *Phys. Rev.* B **74** 195329
[114] Chen L, Xiang H J, Li B, Zhao A, Xiao X, Yang J, Hou J G and Zhu Q 2004 *Phys. Rev.* B **70** 245431
[115] Matsuda I, Liu C, Hirahara T, Ueno M, Tanikawa T, Kanagawa T, Hobara R, Yamazaki S, Hasegawa S and Kobayashi K 2007 *Phys. Rev. Lett.* **99** 146805
[116] Hasegawa S, Shiraki I, Tanikawa T, Petersen C L, Hansen T M, Boggild P and Grey F 2002 *J. Phys.: Condens. Matter* **14** 8379–92
[117] Hasegawa S, Tong X, Jiang C S, Nakajima Y and Nagao T 1997 *Surf. Sci.* **386** 322–7
[118] Hasegawa S and Ino S 1992 *Phys. Rev. Lett.* **68** 1192–5
[119] Henzler M, Luer T and Burdach A 1998 *Phys. Rev.* B **58** 10046–53
[120] Wells J, Song F, Handrup K, Bao S N, Schulte K, Ahola-Tuomi M, Mayor L, Swarbrick J C, Perkins E W and Hofmann Ph 2008 **20** at press
[121] Jiang C S, Hasegawa S and Ino S 1996 *Phys. Rev.* B **54** 10389–92
[122] Jiang C S, Tong X, Hasegawa S and Ino S 1997 *Surf. Sci.* **376** 69–76
[123] Hirahara T, Nagao T, Matsuda I, Bihlmayer G, Chulkov E V, Koroteev Yu M, Echenique P M, Saito M and Hasegawa S 2006 *Phys. Rev. Lett.* **97** 146803
[124] Okino H, Hobara R, Matsuda I, Kanagawa T, Hasegawa S, Okabayashi J, Toyoda S, Oshima M and Ono K 2004 *Phys. Rev.* B **70** 113404
[125] Okino H, Matsuda I, Yamazaki S, Hobara R and Hasegawa S 2007 *Phys. Rev.* B **76** 035424
[126] Petersen C L, Grey F and Aono M 1997 *Surf. Sci.* **377** 676
[127] Pfennigstorf O, Lang K, Gunter H L and Henzler M 2000 *Appl. Surf. Sci.* **162** 537–46
[128] Pfennigstorf O, Petkova A, Guenter H L and Henzler M 2002 *Phys. Rev.* B **65** 045412
[129] Pfennigstorf O, Petkova A, Kallassy Z and Henzler M 2002 *Eur. Phys. J.* B **30** 111–5
[130] Gao B, Chen Y F, Fuhrer M S, Glattli D C and Bachtold A 2005 *Phys. Rev. Lett.* **95** 196802
[131] Novoselov K S, Geim A K, Morozov S V, Jiang D, Zhang Y, Dubonos S V, Grigorieva I V and Firsov A A 2004 *Science* **306** 666–9
[132] Miao F, Wijeratne S, Zhang Y, Coskun U C, Bao W and Lau C N 2007 *Science* **317** 1530–3
[133] Uchihashi T and Ramsperger U 2002 *Appl. Phys. Lett.* **80** 4169–71
[134] Kanagawa T, Hobara R, Matsuda I, Tanikawa T, Natori A and Hasegawa S 2003 *Phys. Rev. Lett.* **91** 036805
[135] Tanikawa T, Matsuda I, Kanagawa T and Hasegawa S 2004 *Phys. Rev. Lett.* **93** 016801
[136] Hirahara T, Matsuda I, Yamazaki S, Miyata N, Hasegawa S and Nagao T 2007 *Appl. Phys. Lett.* **91** 202106
[137] Bunk O, Falkenberg G, Zeysing J H, Lottermoser L, Johnson R L, Nielsen M, Berg-Rasmussen F, Baker J and Feidenhans'l R 1999 *Phys. Rev.* B **59** 12228–31
[138] Yeom H W *et al* 1999 *Phys. Rev. Lett.* **82** 4898
[139] Abukawa T, Sasaki M, Hisamatsu F, Goto T, Kinoshita T, Kakizaki A and Kono S 1995 *Surf. Sci.* **325** 33–44
[140] Kumpf C, Bunk O, Zeysing J H, Su Y, Nielsen M, Johnson R L, Feidenhans'l R and Bechgaard K 2000 *Phys. Rev. Lett.* **85** 4916–9
[141] Gallus O, Pillo T, Hengsberger M, Segovia P and Baer Y 2001 *Eur. Phys. J.* B **20** 313–9
[142] Ahn J R, Byun J H, Koh H, Rotenberg E, Kevan S D and Yeom H W 2004 *Phys. Rev. Lett.* **93** 106401
[143] Park S J, Yeom H W, Min S H, Park D H and Lyo I W 2004 *Phys. Rev. Lett.* **93** 106402
[144] Park S J, Yeom H W, Ahn J R and Lyo I W 2005 *Phys. Rev. Lett.* **95** 126102
[145] Ahn J R, Byun J H, Kim J K and Yeom H W 2007 *Phys. Rev.* B **75** 033313
[146] Sun Y J, Agario S, Souma S, Sugawara K, Tago Y, Sato T and Takahashi T 2008 *Phys. Rev.* B **77** 125115
[147] Tegenkamp C, Kallassy Z, Gunter H L, Zielasek V and Pfnur H 2005 *Eur. Phys. J.* B **43** 557–64
[148] Tegenkamp C, Ohta T, McChesney J L, Dil H, Rotenberg E, Pfnur H and Horn K 2008 *Phys. Rev. Lett.* **100** 076802
[149] Édel'man V S 1976 *Adv. Phys.* **25** 555–613
[150] Issi J-P 1979 *Aust. J. Phys.* **32** 585–628
[151] Ogrin Y F, Lutskii V N and Elinson M I 1966 *JETP Lett.* **3** 71–3
[152] Lutskii V N 1965 *Sov. Phys.—JETP Lett.* **2** 245
[153] Sandomirskii V B 1967 *Sov. Phys.—JETP* **25** 101

[154] Komnik Yu F, Bukhshtab E N, Nikitin Yu V and Andrievskii V V 1971 *Zh. Eksp. Teor. Fiz.* **60** 669–87
[155] Komnik Yu F and Andrievskii V V 1975 *Fiz. Nizk. Temp.* **1** 104–19
[156] Chu H T, Henriksen P N and Alexander J 1988 *Phys. Rev.* B **37** 3900
[157] Hoffman C A, Meyer J R, Bartoli F J, Venere A Di, Xi X J, Hou C L and Wang H C 1993 *Phys. Rev.* B **48** 11431–4
[158] Chu H T 1995 *Phys. Rev.* B **51** 5532–4
[159] Rogacheva E I, Grigorov S N, Nashchekina O N, Lyubchenko S and Dresselhaus M S 2003 *Appl. Phys. Lett.* **82** 2628–30
[160] Sugawara K, Sato T, Souma S, Takahashi T, Arai M and Sasaki T 2006 *Phys. Rev. Lett.* **96** 046411–4
[161] Koroteev Yu M, Bihlmayer G, Gayone J E, Chulkov E V, Blügel S, Echenique P M and Hofmann Ph 2004 *Phys. Rev. Lett.* **93** 046403
[162] Pascual J I *et al* 2004 *Phys. Rev. Lett.* **93** 196802
[163] Hirahara T, Nagao T, Matsuda I, Bihlmayer G, Chulkov E V, Koroteev Y M and Hasegawa S 2007 *Phys. Rev.* B **75** 035422
[164] Nagao T, Sadowski J T, Saito M, Yaginuma S, Fujikawa Y, Kogure T, Ohno T, Hasegawa Y, Hasegawa S and Sakurai T 2004 *Phys. Rev. Lett.* **93** 105501